Efficient DPD Coefficient Extraction For Compensating Antenna Crosstalk And Mismatch Effects In Advanced Antenna System

Md Zahidul Islam Shahin and Himanshu Gaur

Department of Electrical and Information Technology
LTH, Lund University
SE-221 00 Lund, Sweden

Supervisors: Johan Wernehag (LTH, LU)
Liang Liu (LTH, LU)
Raihan Rafique (Ericsson AB)

Examiner: Pietro Andreani

June 5, 2018

Printed in Sweden
Tryckeriet i E-huset, Lund

Abstract

The demand for high data rates in a wireless communication system has experienced a remarkable growth over the last years. This demand is continually increasing with the growing number of wirelessly connected devices. Thus, there is a continuing hunt for increasing the data transmission rate in wireless communication systems.

To increase the data rate, the modern wireless communication system cannot only rely on bandwidth, as usable frequency spectrum is getting crowded. However, advanced antenna system, i.e Multiple input multiple output (MIMO), Multi-user MIMO, massive MIMO, lead to significant advancement in the modern wireless system by increasing data rate, spectrum efficiency, channel capacity, etc. These advanced antenna systems rely on the multi-antenna transmitter, using radio frequency (RF) power amplifiers (PAs) to excite an antenna array. These RF PAs are one of most power consuming devices in a wireless transmitter. Thus, the Energy efficiency of PA is a major concern. Higher efficiency can be achieved by increasing the input power to the PA. However, signals , using modern modulation schemes, like Orthogonal Frequency Division Multiplexing (OFDM) and Wideband Code Division Multiple Access (W-CDMA), have non-constant envelope and high Peak to average power ratio (PAPR). These signals create the conflict between power efficiency and frequency spectrum efficiency (linearity). Linearization techniques such as Digital predistortion (DPD) is most widely used to linearize the PA so that it can be driven in high power mode for maximizing energy efficiency.

However, the coupling between array elements modulate the load on the output of each PA, creating post-PA crosstalk. Thus, Power Amplifier behaviour changes which affect the DPD linearization of the PAs since DPD technique is performed without considering these coupling effects. Thus, some degradation of the system performance in terms of linearity is expected. To address this problem, PA linearization techniques have been explored in this thesis. This thesis work is related to the field of research towards a study of post-PA crosstalk effects and exploring a solution to compensate for both non-linearity and crosstalk at the output of the power amplifier.

To emulate multi-antenna transmitter system, a uniform linear array with four transmit antennas and four PAs is built in this thesis. Digital beamforming technique is applied to the antenna array to mimic advanced antenna system. The coupling between array elements is extracted using S-parameters of the array elements. There is no significant impact found on PA output signal Adjacent channel power while post-PA crosstalk is present but without DPD. However, the impact of post-PA crosstalk found on DPD linearization performance.

A simulation model is developed using static behavioural PA models in crosstalk environment and extracted S-parameter from the array antenna. The simulation using conventional DPD in crosstalk environment shows around 30dB degradation of linearization performance in the high coupling scenario.

An algorithm called Crosstalk Digital Preistortion (CDPD) is developed and proposed in this thesis to compensate crosstalk effects on DPD. The proposed solution is tested in a simulation environment. The simulation results show that the proposed method improves the DPD linearization performance about 25dB under the very high coupling scenario. The new algorithm also improves the performance in extracting the model parameters for digital Predistortion in a multi-antenna system.

Acknowledgement

We would like to express our gratitude to the people who guided and helped us during the thesis. Without the guidance and help of those people, it would not be easy to complete the thesis successfully.

First of all, We would like to express our gratitude towards our supervisor in Ericsson, Raihan Rafique, for his continuous guidance and support throughout the thesis. His help, guidance and continuous support made the thesis work easier.

Secondly, We would like to thank our main supervisor, Johan Wernehag, at Lund University, for his smooth explanation of the questions that we asked and for the proper guidelines to finish the thesis. We would also like to express our gratitude to our supervisor, Liang Liu at Lund University, for his fruitful input and detailed explanation of several issues that we encountered while doing the thesis.

Thirdly, We would like to thank Hans Hagberg at Ericsson for explaining several technical issues clearly. We are really thankful to Åke Kristoffersson, Lab supervisor at Ericsson, for his time, guidance and providing us with all instrument that we need to properly do the thesis work. We are really grateful towards Housam Elfeituri at Ericsson for his continuous support in 3D printing. We want to thank Jacob Mannerstråle, manager at Ericsson, for giving us this valuable opportunity to do the thesis at Ericsson and also to provide us with all necessary support.

Finally, we express our gratitude to our parents. From our childhood, their support in our education made it possible to come this long way.

Table of Contents

List of Figures

List of Tables

Acronyms

PA : Power Amplifier
DPD : Digital Pre-Distortion
CDPD : Crosstalk Digital Pre Distortion
ACLR : Adjacent Channel Leakage Ratio
ACPR : Adjacent Channel Power Ratio
PAPR : Peak to Average Power Ratio
AAS : Advanced Antenna System
LTE : Long Term Evolution
MIMO : Multiple Input Multiple Output
NMSE : Normalized Mean Squared Error
PAE : Power Added Efficiency
SNR : Signal to Noise Ratio
WCDMA: Wideband Code Division Multiple Access
IoT : Internet of Things
MU-MIMO : Multi-user MIMO
UE : User Equipment
OFDM : Orthogonal Frequency Division Multiplexing
RF : Radio Frequency
CO-MPM: Cross-over Memory Polynomial Model
E-PHEMT: Enhancement-mode High Electron Mobility Transistor
AM-AM : Amplitude to Amplitude
AM-PM : Amplitude to Phase
ISM: Industrial, Scientific, and Medical radio band
PIFA: Planar Inverted-F Antenna
ULA : Uniform Linear Array
AF : Array Factor
HPBW: Half Power Beam width
LO : Local Oscillator
EM : Electromagnetic
VNA: Vector Network Analyzer
S-parameters: Scattering Parameters
3GPP: 3rd Generation Partnership Project

Popular Science Summary

The modern wireless communication system is growing fast with the advent of 5G and IoT development. This has pushed the data rate limits higher than ever before, further pushing the need for higher bandwidth requirements. Multiple Input Multi-Output (MIMO) technology which uses LTE (4G communication) signals evolved to address the issue. But for MIMO systems, with a large array of antennas closely packed in a small area, emitting signals of the same frequency, at the same time and using antenna processing technique such as beamforming, a new problem of Radio Frequency (RF) system, called crosstalk, becomes significant.

Some of the signals transmitted by one antenna can be received by other transmitting antennas and this can affect the signal emitted by the first antenna. This is referred to as coupling between antennas. Due to the close proximity to each other coupling between antennas become dominant. This can result in post-PA crosstalk effects. Indeed the coupling between two antennas may reach high coupling under certain conditions.

Crosstalk may also lead to signal distortion and nonlinearity. This crosstalk effect has to be addressed for next generation of wireless systems and for cellular communications in the mmWave 5G system. The motivation is to improve Power Amplifier performance for the development of efficient and low-cost small cell radio base station that can be used in a future 5G system. This means, there is a necessity for a robust algorithm to compensate for these effects in the 5G system for better system performance.

This thesis studies the distortions at the power amplifier output in MIMO transmitters considering the post-PA crosstalk effects and proposes a Digital Pre-Distortion based solution to compensate for the aforementioned crosstalk effects.

Chapter 1
Introduction

This chapter is divided into seven sections: Background and motivation, project aims and main challenges, approach and methodology, previous work, limitations, resources and thesis outline.

1.1 Background and Motivation

Over the past few years, we were experiencing how our day-to-day lives were transformed through the Internet of things (IoT) connected devices, sensors and other parallel infrastructures. It has already been projected that roughly over 50 Billion IoT devices will be connected by 2020, followed by a mobile data traffic increase of 24.3 Exabyte per month by 2019 [11]. It is obvious that, in the future, we will need a massive data rate as well as the more advanced wireless solution to support IoT and other parallel infrastructures.

Modern wireless communication standards like LTE and future 5G will be the access technology for IoT. To fulfil the demand of higher data rate, the cellular communication system cannot only rely on bandwidth as usable frequency spectrum is getting crowded. In this regard, advancement in the field of antenna systems plays a significant role in the current modern wireless system.

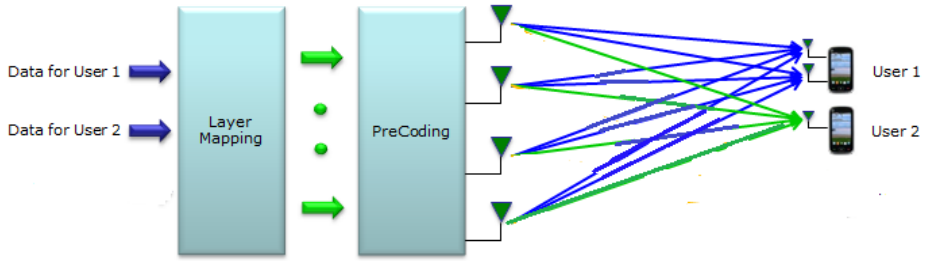

Figure 1.1: MU-MIMO [1]

MIMO system has already become an essential part of modern wireless communication system systems like LTE and IEEE 802.11n. Moreover, progress in MIMO leads to Massive MIMO and MU-MIMO system, which are the most promising technology for the future next-generation wireless systems. These advanced antenna system has marked a

significant improvement in the modern cellular system by increasing data rate, spectrum efficiency, channel capacity, mitigating multi-path fading and reducing the co-channel interference [38].

In the multi-user communication system, base station utilizes multiple antennas and beamforming technique to transmit multiple user data streams in the downlink. A sample MU-MIMO system [15], serving at least or more than 2 UEs simultaneously, is shown in Fig. 1.1. For 5G Radios, due to a small cell area, the number of deployed units is always going to be high. Thus, technology advancement for efficient, low power and low-cost small cell radio base station is in high demand. Power amplifier efficiency and performance is of great concern for overall system performance of small cell radio with advanced Antenna System (AAS).

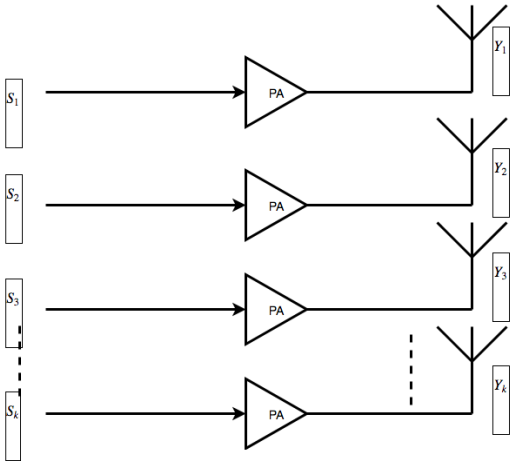

Figure 1.2: Multi-antenna transmitter system model with K transmit paths

In Multi-antenna system, each transmit path has its own power amplifier (PA) and antenna element as shown in Fig. 1.2. Power Amplifiers (PA) are one of the most important blocks, which is responsible for overcoming the loss of the signal power between the transmitter and receiver. Thus, high efficiency is required for the PA. Current wireless and cellular system such as LTE, LTE advanced and some standard of IEEE 802.11 are using complex modulation and multiple access techniques, i.e. Orthogonal Frequency Division Multiplexing (OFDM) [22] with high peak to average power ratio (PAPR) for better spectrum efficiency. High input power can improve the efficiency, on the other hand, PA non-linear problem arises due to high PAPR. With high power, PA inherently behaves non-linearly that results in the violation of 3GPP standards [28], which defines the maximum acceptable Adjacent Channel Power Ratio (ACPR) and absolute adjacent leakage power for the mobile phone communications standards e.g. 3G, LTE (4G). Linearization of PA is essential for these standards to maintain ACPR within an acceptable limit. One of the most widely used and effective technique for PA linearization is the Digital Pre-Distortion (DPD) technique.

Large-scale multi-antenna system, comprising up to several hundreds of transmit paths along with advanced antenna techniques, introduces several challenges on DPD

implementation. Crosstalk between the multiple paths is one of the main challenges. Crosstalk or coupling effects are the result of signal interferences from two or more sources [7, 31]. In MIMO transceivers, crosstalk originates from the interference or coupling between the different transmitter paths. Since many antennas are transmitting at the same frequency, array elements are coupled. The coupling creates variable loads at the output of each PA, which changes the load line characteristics of the PA [34]. As a result, in the multi-antenna system, the behavior of each PA is dependent on the coupled signal from the other array antenna elements. The effect of crosstalk between antennas can also be prevented by insulators, which not only introduce losses, but also does not fit in typical modern IC transmitter designs.

Current DPD linearization of the RF PAs is performed without considering these coupling effects. Thus, some degradation of the system performance in terms of linearity is expected, which needed to be addressed in the next generation massive MIMO based wireless system.

1.2 Project Aims and Main Challenges

The aims of this master's thesis work are listed below:

- Build a test setup to mimic advanced antenna system using a 4X1 Linear array with digital beamforming technique.
- Investigate power amplifier characteristics and nonlinear behaviour using PA measurements.
- Study DPD algorithms and investigate DPD performance using measurement setup.
- Create PA behavioural model from physical PA measurement.
- Investigate and analyze different crosstalk problems using test setup measurements.
- Investigate Antenna coupling and S-parameters of an array.
- Build a simulation model to represent the setup and find a solution for crosstalk effect compensation using DPD.
- Test the proposed solution using measurement setup to observe the linearization performance in crosstalk environment.

There are several challenges of the thesis work. Those challenges are listed below:

- To build the test setup with available PAs and antennas.
- To generate coherent signals due to unavailability of the license feature of the instrument.
- To find a solution to compensate crosstalk effect with DPD.
- Building the array with the available antennas. The array is not in good shape due to antenna plane misalignment and the mismatch between antennas.
- Interfacing between Simulation and measurement setup.

1.3 Approach and Methodology

The flow diagram of approach and methodology used in this master's is given below:

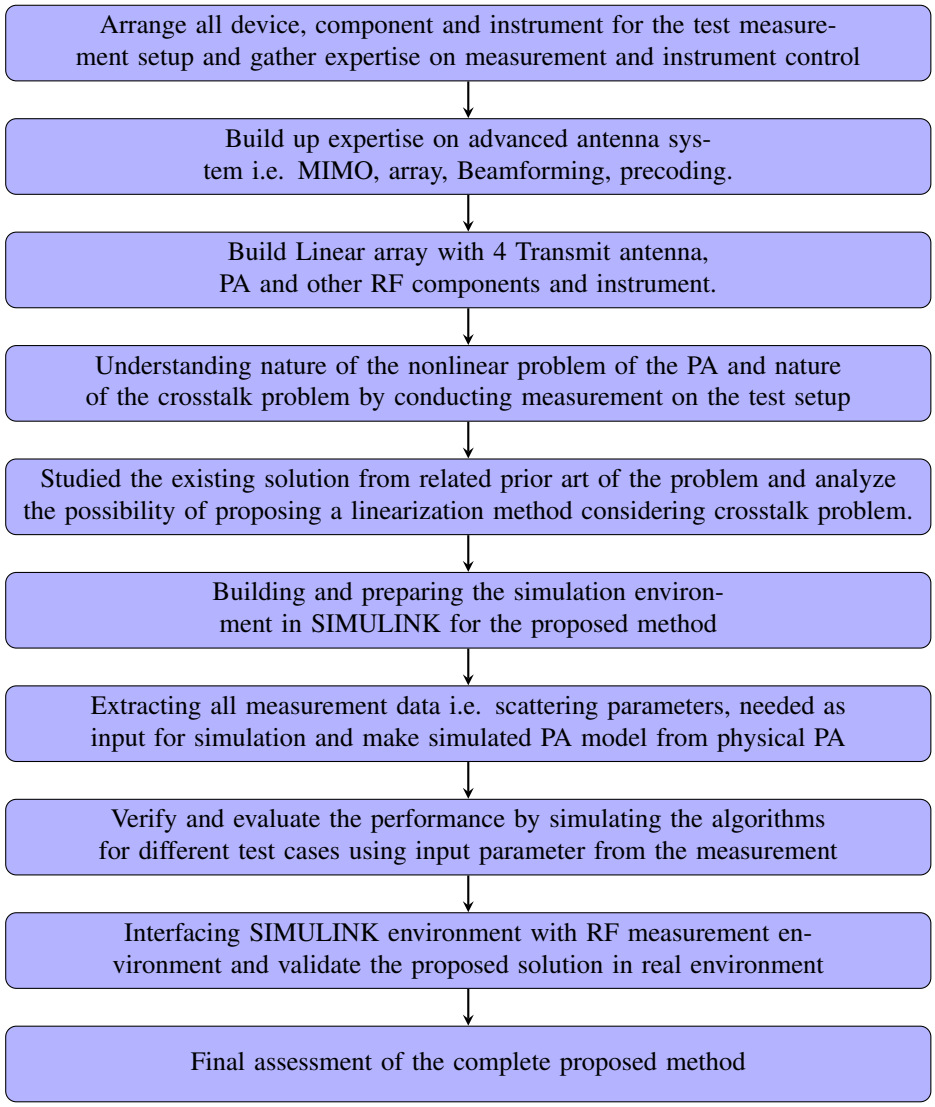

To be able to investigate the real world behaviour of the multi-antenna setup, measurement was taken using built-in MATLAB functions and necessary toolbox needed for instrument control. The simulation environment was created using Simulink to perform the investigations needed to reach the goals of this thesis. During this process a good understanding was built upon RF measurement and instrument control, design and implementation of smart antenna system, simulation framework, system model.

1.4 Previous Works

The cause and behavior of nonlinear distortion of PA, finding linearization method and crosstalk have been important topics in research for many years. Many solutions, methods and approaches have been proposed for PA linearization of multiple antenna transmitters with crosstalk distortion compensation.

In [7], crossover memory polynomial model (CO-MPM) and DPD structures for wideband signals approximating the output of a MIMO power amplifier (PA) as the sum of two nonlinear functions considering crosstalk before PA, was proposed. These methods are not enough as they lack cross-products between signals of different transmit paths. In [2],a method was proposed considering certain cross-products. In [3], a model and predistorter structures were proposed, including memory effects to characterize and linearize crosstalk before the PA. In [16], a linearization technique called MIMO-PD based on recursive algorithms with reduced computational complexity was proposed to compensate nonlinear distortion due to crosstalk before PA. However, all these proposed methods consider the before PA crosstalk in their linearization method and rely on measurements of all individual transmitter output signals for the identification of the proposed models and predistorters.

In [9], the impact of multi-antenna coupling and mismatch on the PA output signal has been investigated. In [37], the effects of mutual antenna coupling and mismatches on the behavior of PAs using a dual-input PA model with measurement of antenna array scattering characteristics (S-parameters) was investigated. The impact on PA due to source and load mismatch, a dual-input PA model structure was presented in [45]. In [6], a DPD method for highly correlated input signals, as in phased arrays and beam-steering applications, was proposed.

1.5 Resources

This thesis work was conducted at Ericsson, Lund under Business Unit Radio Access Department. A workbench was provided in the Radio lab. Two computers were also provided with MATLAB bound to a professional license. RF instruments like Signal Analyzer, Signal generator, RF switch, Digital Oscilloscope, DC power source and all other RF components in the LAB were provided by Ericsson AB.

1.6 Thesis Outline

After the introductory chapter, the remainder of thesis work is organized into 8 chapters. In Chapter 2, firstly, power amplifier basics, PA measurement test results for characterization and PA nonlinear behavior are presented. Chapter 3 discusses PA behavioral modelling approaches and DPD basics with the architectures. In chapter 4, the antenna array, basics of array synthesis, beamforming method and setup of 4X1 Linear array antenna will be discussed. Thereafter, multi-antenna system modelling for different crosstalk scenario, mutual coupling of antenna arrays and effect on PA output signal due to crosstalk are discussed. Later, in chapter 6, the proposed approach with crosstalk DPD algorithm will be presented. Thereafter, simulation results with the proposed method and performance of

the method are discussed in chapter 7. Finally, Chapter 8 concludes summarizing major outcomes and chapter 9 highlights some future works.

Chapter 2
Power Amplifier Characterization

This chapter is divided into several sections. At first, PA role in the wireless link and PA basics are discussed. The PA, which is used for the project, is presented in the next section. Thereafter, PA properties and different PA behaviors are discussed. Finally, PA non-linear behavior and impact on signal distortion are presented.

2.1 Power Amplifier and Wireless Transmission Link

The power amplifier (PA) is an essential components in wireless communication systems. The Fig. 2.1 shows a block diagram of wireless transmitter. Enough transmission power is required to mitigate the loss between the transmitter and receiver. Hence, PAs are used to amplify the signal of the communication link in order to deliver with enough power so that signal can be properly detected by the receiver. Since PA is the most power hungry devices of the transmission link, it is considered as a crucial and a major component in transmitter design.

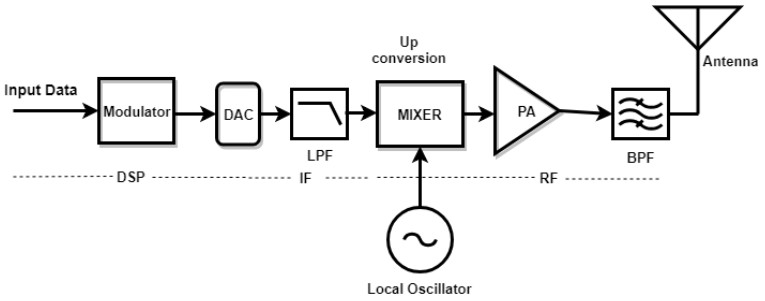

Figure 2.1: Simplified block diagram of transmitter

2.2 PA Basics

RF power amplifier is a type of electronic amplifier that converts a low-power RF signal into a high power signal without adding any change to the format, modulation, or other factors. It amplifies the signal before antenna transmission without creating too much

noise. It also limits the amplification of the signal within the desired bandwidth as much as possible.

2.3 PA Under Test

2.3.1 PA Device Description

The power amplifier that is used for this project is shown in Fig. 2.2. It is a Mini-circuits System In Package (MSiP) surface mount IC (model no: YSF-322+), made of GaAs with E-PHEMT. It provides a maximum 1.5 W. The choice of such PA was made because it is suitable for cellular applications such as LTE. The PA provides a strong combination of performance parameters, including high gain (20 dB), high IP3 (+35 dBm) and P1dB (+20 dBm), low noise figures (2.8dB) and broad frequency range covering 900 MHz to 3.2GHz. A Suitable module, shown in Fig. 2.3, was made from the IC to operate the PA according to the measurement need.

Figure 2.2: Power Amplifier IC

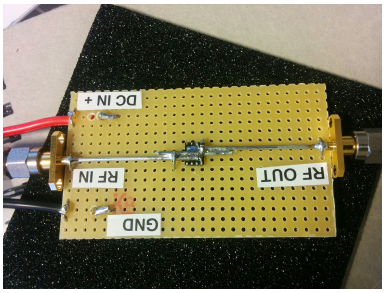

Figure 2.3: Power Amplifier module

2.3.2 Frequency

ISM band wifi antenna, which has a peak gain at 2.44 GHz, will be used in over the air measurements. Thus, 2.44 GHz is chosen as carrier frequency in all measurements. PA can be considered as wideband covering 900 MHz to 3.2GHz.

2.3.3 PA Test setup

A simple measurement setup using a sinusoidal RF signal source (single tone) consists of a network analyzer, PA and DC power source is shown in Fig. 2.4. This is single tone measurement setup for PA test. Furthermore, PA test is required for 20MHz LTE signal as it will be used for all future measurements. Multi-tone test setup for LTE signal is shown in Fig. 2.5.

The measurement results using these setups will be discussed in later sections.

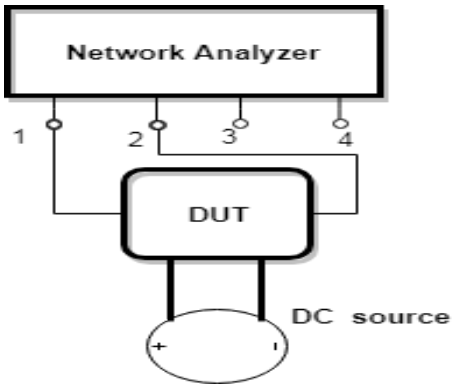

Figure 2.4: Single tone measurement setup

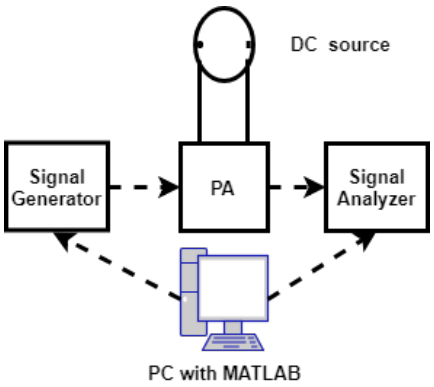

Figure 2.5: Multi-tone measurement setup

2.4 Power Amplifier Characteristics

2.4.1 Gain and Gain Compression

The Gain of a power amplifier is defined by the ratio between the output power and the input power given in (2.1).

$$Gain = 10log_10(\frac{P_out}{P_in}) \tag{2.1}$$

The gain is dependent on many factors such as properties of the amplifier's different transistors, input power, frequency and other input parameters. However, over a certain bandwidth and the input power range, the gain can be considered as constant. The gain of the PA is no longer constant at compression point. To describe the gain compression, first dB compression point (P1dB) is used. P1dB is defined as the input power for which the real PA gain is 1dB lower than the theoretical linear slope of constant gain.

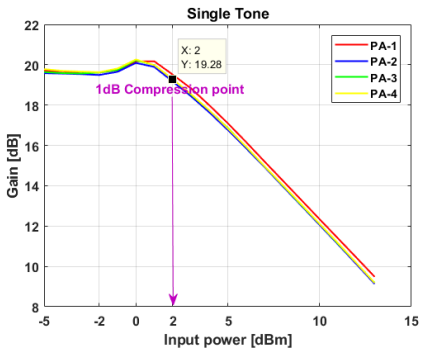

Figure 2.6: input power vs Gain

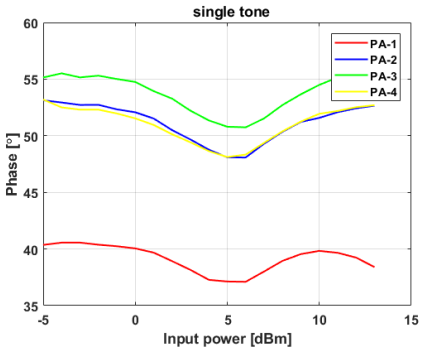

Figure 2.7: Input power vs Phase

The Fig. 2.6 shows the measured results of the single tone setup as shown in Fig. 2.4.

It can be seen from Fig. 2.6 that the four PAs, that has been used in the project, have similar gain characteristics and approximately same compression point. All four PAs also have similar phase response which is shown in Fig. 2.7. The gain and phase characteristics of all the four PA are found almost same in the single tone test. The compression point is found at +2dBm input power for the single tone.

Moreover, the PA test results of multi-tone setup (Fig. 2.5) are drawn in Fig. 2.8 and Fig. 2.9. The Fig. 2.8 shows that the gain characteristics for 20MHz LTE signal are almost similar for all four PA. The input power vs output power plot in Fig. 2.9) also approximately same for all four PA. It is noted that the compression point is backed off to -2dB for all four PA. This is because the signal is an LTE signal having an 8dB peak to average power ratio (PAPR) with 20MHz bandwidth.

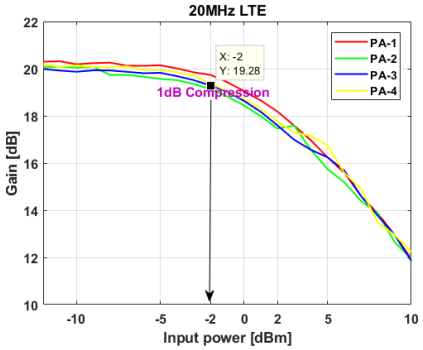

Figure 2.8: Input power vs Gain

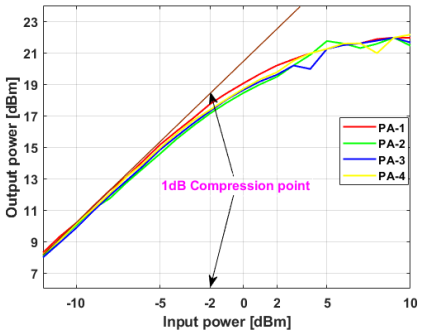

Figure 2.9: Input vs Output power

As all the four PA are behaving in a similar fashion, these pies are suitable for multi-antenna transmitter setup.

2.4.2 Trade-off between Linearity and Energy Efficiency

The power amplifier is one of the most power consuming devices. Thus, the Energy efficiency of PA is a major concern in a wireless transmitter. Power added efficiency (PAE) [32] is commonly used to measure the energy efficiency of the PA.

Higher efficiency can be achieved by increasing the input power to the PA [32]. Modern communication techniques use latest modulation scheme like W-CDMA and OFDM. These modulation scheme has non-constant envelope and high PAPR. Signals with high PAPR creates the conflict between power efficiency and linearity. If PA is operated in non-linear region, frequency spectral regrowth is observed due to harmonic distortion products.

However, due to strict frequency allocations, this spectral regrowth problem need to be tackled [28]. Violation of these allocations is strictly prohibited for any wireless communication technique for any carrier frequency. Efficiency is needed to lower the power consumption. On the other hand, If PA is run in compression region, the nonlinear behaviour start to increase. This problem lead to unavoidable trade-off between efficiency and linearity.

2.4.3 Power Amplifier Nonlinearity

As discussed in the previous section, there is a trade-off on selecting the operating point of a PA. To have maximum output power, PA needs to be operated in the nonlinear or saturation region. However, PA nonlinear properties become prominent in their saturation region. Power amplifier nonlinearity can be investigated from the characteristics of amplitude to amplitude (AM/AM) conversion and amplitude to phase (AM/PM) conversion.

2.4.3.1 AM/AM and AM/PM Characteristic

RF PA operates in a certain limited band, and they are baseband in nature. It is flexible to use complex envelop notation to describe the RF PAs [27]. If the input signal to a PA is [27],

$$x(t) = a(t)e^{j\varphi(t)} \tag{2.2}$$

Where, $a(t)$ is the envelope and the $\varphi(t)$ is the phase of the input signal. The output response of the nonlinear PA i.e. $y(t)$ will be the amplified distorted version of the $x(t)$. The output can be represented as[27],

$$y(t) = g[a(t)]e^(j\varphi(t) + f(a(t)) \tag{2.3}$$

Whereas, function g and f appears due to the non-ideal behavior of the PA and denoted as Amplitude to Amplitude (AM/AM) and Amplitude to Phase (AM/PM) distortion[27]. AM/AM distortion can be defined as the deviation from the constant gain when PA is operated in compression region. On the other hand, the increased phase change at compression region can be termed as AM/PM distortion. AM/AM and AM/PM response using LTE 20MHz signal are shown in Fig. 2.10 and Fig. 2.11 respectively.

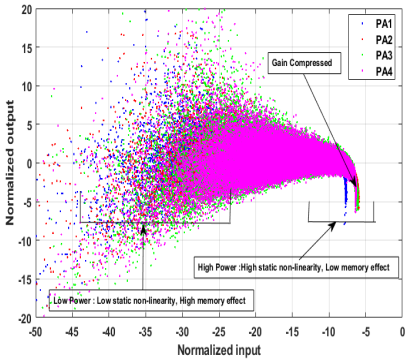

Figure 2.10: AM-AM

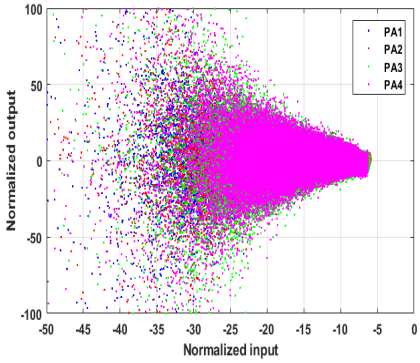

Figure 2.11: AM-PM

In presence of wideband signals having non constant amplitude, PA behaves as nonlinear system and exhibits two types of nonlinearities; static distortion and memory effects [29].

In Fig. 2.9, 1dB compression point is shown, where RF input power and RF output power relation is not linear. The peak of high PAPR signal force the PA to run in compression region. Thus , the gain deviation from constant value and increment of phase change

is observed. Fig. 2.10 and Fig. 2.11 shows AM/AM and AM/PM distortion respectively at comression point of the PA. This is static distortion. Further, due to transistor characteristic, PA shows the memory effect distortion[29]. The memory effect in an amplifier caused by thermal and electrical memory. The memory effects results delay effect, filtering effects in transistors. Circuit response to modulated waveforms is unpredictable due to memory effect. The memory effect can be seen in Fig. 2.10. At low power, the memory effect is significant and the samples are too spread. On the other hand, at high power memory effect is hard to detect as the gain compressed.

Compressed peaks due to static nonlinerity at time domain as shown in Fig. 2.10 has a spectral growth effect in frequency domain. The adjacent channel power of the transmitted signal start to increase due to spectral growth.

2.4.4 Impact of PA Nonlinearity

Due to spectral regrowth, PA nonlinear behaviour has a severe impact on signal out-of-band power. Adjacent channel Leakage ratio (ACLR) and adjacent channel power ratio (ACPR) represent the same thing. It is a measure of the power of the distortion components that are leaked into the adjacent channel. The ACLR is defined as the ratio of the power of a signal leaked in the signal bandwidth of the adjacent channel to the power of the same signal emitted in the signal bandwidth of the main channel [41]. Mathematically, ACLR is defined as [41],

$$ACLR_{dB} = 10log_{10}\frac{\int_{adjch}|Y(f)|^2df}{\int_{mainch}|Y(f)|^2df} \tag{2.4}$$

where, $Y(f)$ is the Fourier transform of the signal, $adjch$ and $mainch$ represent the signal bandwidth of the adjacent and main channel respectively.

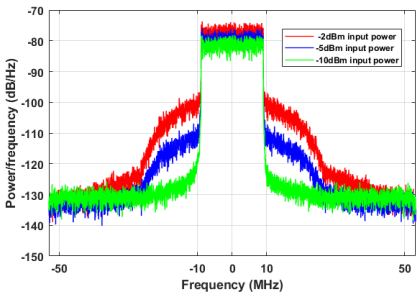

Figure 2.12: Power Specteal density vs Input power

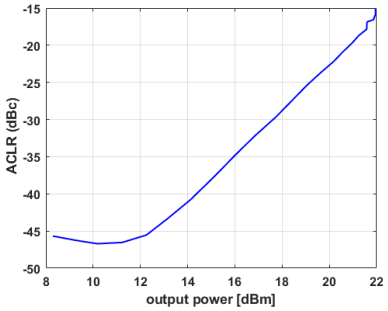

Figure 2.13: ACLR vs Output power

Due to Spectral regrowth, ALCR of the PA output signal increases. The degradation or increase of ACLR level can be seen in Fig. 2.12 and Fig. 2.13. In Fig. 2.13, the ACLR increases as the PA output power increases. The increase is too sharp and significant in compression or nonlinear region of the PA.

Similar observation can be found in Fig. 2.12 where power spectral densities (PSD) [41] of output signals from PA are plotted for the different level of input power using

20 MHz LTE signal. For high input power level (-2 dBm) the PA response shows high spectral growth compared to the lower input power level (-10 dBm).

The design of PA and transmitter is going to be a challenge due to increase in bandwidth demand and at the same time requirement of high linearity and efficiency. We can back-off the input signal to fulfill the linearity requirement of the power amplifier. However, the power amplifier efficiency will be very low for high PAPR signals. Another choice is to linearize a nonlinear power amplifier so that overall we have a linear and reasonably efficient device. Linearization techniques are used both to improve linearity and efficiency. Digital predistortion is one of the most widely used and cost-effective techniques among all linearization techniques [32].

Chapter 3

PA Modelling And Digital Predistortion

3.1 PA Modeling

To emulate the effects of physical power amplifiers in a simulation model, mathematical models of power amplifiers used in measurement setup are required. For this reason, PA modeling is required, and the approach adopted in the thesis has been presented here.

An ideal tool for the system level simulation is required, for this reason, the behavioral modeling approach is adopted here. Behavioral modeling regards the internal structure of a PA as a black box and relies only on the observation of input and output signals of the PA. It is built and tuned by a mathematical expression such as to make the output of the model match with the measured output of the PA with the same input signals. From a computational complexity point of view, behavioral modeling is an efficient solution and it is easier to implement the model on computational devices. Only the input and output signals of the PA are required, instead of delving into sophistication inside the PA's internal structure. Model accuracy, the computational complexity, and the model extraction technique are the main criteria based on which selection of behavioral model is dependent upon.

Modeling approach for the power amplifiers has been presented here. A memory polynomial expression derived from the Volterra series [3.1.1] models the nonlinear relationship between input and output signals. The power amplifier includes memory effects because the output response depends on the current input signal and the input signal at previous times. These power amplifiers are useful when transmitting wideband or narrowband signals.

3.1.1 Full Voltera Model

The Volterra model [40][8] provides a general way to model a nonlinear system with memory which is a combination of linear convolution and nonlinear power series. It is considered as an extension of the Taylor series. In this model, the relationship between the input and output signals is:

$$y(n) = \sum_{p=1}^{P} \sum_{i_1=0}^{M} \dots \sum_{i_p=0}^{M} h_p(i_1, ..., i_p) \prod_{j=1}^{p} x(n - i_j) \tag{3.1}$$

where x(n) and y(n) are the input and output signals, respectively, $h_p(i_1, ..., i_p)$ are the coefficients of the Volterra model, often called Volterra kernels, P is the nonlinearity order of the model, and M is the memory depth.
We can improve accuracy of the model by increasing P and M. Unfortunately, this high accuracy is obtained at the cost of unnecessary computational complexity since the number of parameters will grow exponentially. Nevertheless, the Volterra model is well suitable for modeling dynamic nonlinear behavior [21].

3.1.2 Modeling Process

Figure 3.1 shows the modeling process adapted to model the PA's from a set of four physical PA's, used in the measurement set up of 4x1 MIMO in the thesis.

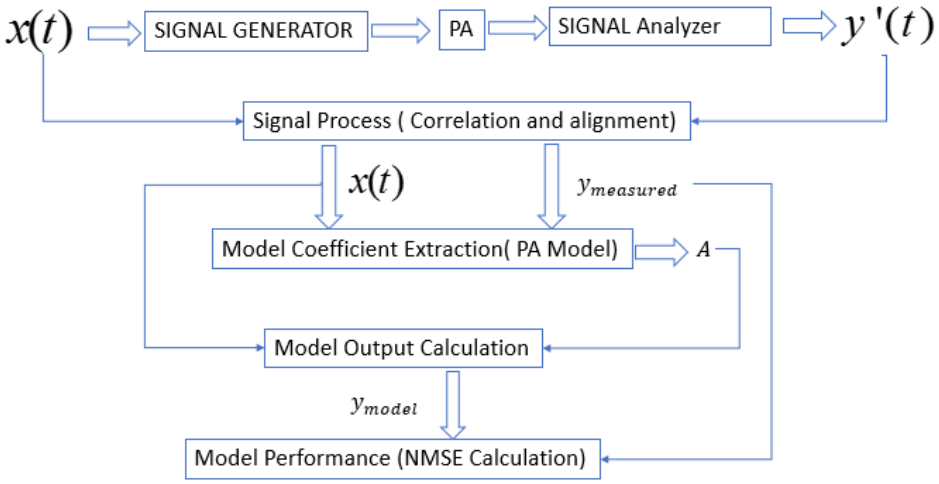

Figure 3.1: PA Modeling Process[42]

3.1.3 Memory Polynomial Model for Power Amplifier

The memory polynomial model [14][23][13][10] has been widely used as a behavioral modeling in digital predistortion of PAs with memory effects. It corresponds to a reduction of the Volterra series in which only diagonal terms are kept. It has a reasonable compromise between computational complexity and model accuracy. The output waveform of the model is given by Eqn (3.2)

$$y_{MP}(n) = \sum_{k=0}^{K-1} \sum_{m=0}^{M-1} C_{km} V(n - m)|V(n - m)|^k \tag{3.2}$$

where $V(n)$ and $y_{MP}(n)$ are the input and output signals, respectively, K is the nonlinear order, M is the memory depth and C_{km} are the model coefficients. This memory polynomial implementation [25] operates on the envelope of the input signal, does not generate new frequency components, and captures in-band spectral regrowth. This model is used to create a wideband amplifier operating at high frequency.

The output signal, at any instant of time, is the sum of all the elements of the following complex matrix of dimensions $MemoryDepth(mem) * VoltageOrder(deg)$:

$$y_{MP}(n) = \begin{bmatrix} C_{11}V_0 & C_{12}V_0|V_0| & ... & C_{1,deg}V_0|V_0|^{deg-1} \\ C_{21}V_1 & C_{22}V_1|V_1| & ... & C_{2,deg}V_1|V_1|^{deg-1} \\ ... & ... & ... & ... \\ C_{mem,1}V_{mem-1} & C_{mem,2}V_{mem-1}|V_{mem-1}| & ... & C_{mem,deg}V_{mem-1}|V_{mem-1}|^{deg-1} \end{bmatrix} \tag{3.3}$$

In the matrix, the number of rows equals the number of memory terms, and the number of columns equals the degree of the nonlinearity. The signal subscript represents amount of delay.

3.1.4 Cross Term Memory Model for Power Amplifier

As mentioned above, the memory polynomial model is a simplified case of Volterra model which eliminates all the cross memory parts. However, as the the signal bandwidth has significantly increased, the memory polynomial model is not enough and the introduction of the cross terms in the full Volterra model is needed. A generalized form of the kth memory polynomial component in Eqn (3.2) can be written by inserting a local delay of m samples between the signal and its exponential part. The delay could be both positive and negative. If we add both these positive and negative local memory that close to the current memory to the typical memory polynomial model in Eqn (3.2), it will come out the generalized memory polynomial model Eqn (3.4) [25].

$$\begin{aligned} y_{GMP}(n) = & \sum_{k=0}^{K_a-1}\sum_{l=0}^{L_a-1} a_{kl}V(n-l)|V(n-l)|^k + \\ & \sum_{k=1}^{K_b-1}\sum_{l=0}^{L_b-1}\sum_{m=1}^{M_b} b_{klm}V(n-l)|V(n-l-m)|^k + \\ & \sum_{k=1}^{K_c-1}\sum_{l=0}^{L_c-1}\sum_{m=1}^{M_c} c_{klm}V(n-l)|V(n-l+m)|^k \end{aligned} \tag{3.4}$$

where the first part is the same as memory polynomial model, while the last two terms are the cross memory with both positive and negative time shifts. K_a and L_a, K_b and L_b, K_c and L_c are the polynomial order and memory depth for the current, positive and negative parts, respectively, M_b and M_c are the local memory that shift from the current memory. The generalized memory polynomial model can be seen as the advanced version of the memory polynomial model. It has a better performance, in terms of reducing spectral regrowth, than the memory polynomial model. However, it suffers a problem of higher computational complexity [21].

This generalized memory polynomial implementation [25] operates on the envelope of the input signal, does not generate new frequency components, and captures in-band spectral

regrowth. This model is used to create an amplifier operating at high frequency. The model includes leading and lagging memory terms and provides a generalized implementation of the memory polynomial model.

The output signal, at any instant of time, is the sum of all the elements of a matrix specified by the element-by-element product $C.*M_{CTM}$ where C is a complex coefficient matrix of dimensions
$MemoryDepth(mem) * MemoryDepth(mem)(VoltageOrder(deg) - 1) + 1$ and

$$M_{CTM} = \begin{bmatrix} |V_0| \\ |V_1| \\ ... \\ V_{mem-1} \end{bmatrix} \begin{bmatrix} 1 & |V_0| & |V_1| & ... & |V_{mem-1}| & |V_0|^2 & ... & |V_{mem-1}|^2 & ... & |V_0|^{deg-1} & ... & |V_{mem-1}|^{deg-1} \end{bmatrix} \tag{3.5}$$

$$= \begin{bmatrix} V_0 & V_0|V_0| & V_0|V_1| & ... & V_0|V_{mem-1}| & V_0|V_0|^2 & ... & V_0|V_{mem-1}|^2 & ... & V_0|V_0|^{deg-1} & ... & V_0|V_{mem-1}|^{deg-1} \\ V_1 & V_1|V_0| & V_1|V_1| & ... & V_1|V_{mem-1}| & V_1|V_0|^2 & ... & V_1|V_{mem-1}|^2 & ... & V_1|V_0|^{deg-1} & ... & V_1|V_{mem-1}|^{deg-1} \\ ... & ... & ... & ... & ... & ... & ... & ... & ... & ... & ... & ... \\ V_{mem-1} & V_{mem-1}|V_0| & V_{mem-1}|V_1| & ... & V_{mem-1}|V_{mem-1}| & V_{mem-1}|V_0|^2 & ... & V_{mem-1}|V_{mem-1}|^2 & ... & V_{mem-1}|V_0|^{deg-1} & ... & V_{mem-1}|V_{mem-1}|^{deg-1} \end{bmatrix} \tag{3.6}$$

In the matrix, the number of rows equals the number of memory terms, and the number of columns is proportional to the degree of the nonlinearity and the number of memory terms. The signal subscript represents amount of delay. The additional columns that do not appear in the Memory polynomial model represent the cross terms.

3.1.5 Coeffcients Extraction

To compute coefficient matrices, the an overdetermined linear system of equations needs to be solved. Consider the Memory polynomial model for the case where the memory length is 2 and the system nonlinearity is of third degree. The matrix that describes the system is

$$\begin{bmatrix} C_{11}V_0 & C_{12}V_0|V_0| & C_{13}V_0|V_0|^2 \\ C_{21}V_1 & C_{22}V_1|V_1| & C_{23}V_1|V_1|^2 \end{bmatrix} \tag{3.7}$$

and the sum of its elements is equivalent to the inner product of

$$\begin{bmatrix} V_0 & V_1 & V_0|V_0| & V_1|V_1| & V_0|V_0|^2 & V_1|V_1|^2 \end{bmatrix} \begin{bmatrix} C_{11} \\ C_{21} \\ C_{12} \\ C_{22} \\ C_{13} \\ C_{23} \end{bmatrix} \tag{3.8}$$

If the input to the amplifier is the n-sample signal [x(1) x(2) ... x(n-1) x(n)] and the corresponding output is [y(1) y(2) ... y(n-1) y(n)], then the solution to

$$\begin{bmatrix} x(2) & x(1) & x(2)|x(2)| & x(1)|x(1)| & x(2)|x(2)|^2 & x(1)|x(1)|^2 \\ ... & x(2) & ... & x(2)|x(2)| & ... & x(2)|x(2)|^2 \\ x(n-1) & ... & x(n-1)|x(n-1)| & ... & x(n-1)|x(n-1)|^2 & ... \\ x(n) & x(n-1) & x(n)|x(n)| & x(n-1)|x(n-1)| & x(n)|x(n)|^2 & x(n-1)|x(n-1)|^2 \end{bmatrix} \begin{bmatrix} C_{11} \\ C_{21} \\ C_{12} \\ C_{22} \\ C_{13} \\ C_{23} \end{bmatrix} = \begin{bmatrix} y(2) \\ ... \\ y(n-1) \\ y(n) \end{bmatrix} \tag{3.9}$$

which can be found using psedoinverse, this provides an estimate of the coefficient matrix. The treatment of the Cross-Term Memory model is similar. The matrix that describes the

system is

$$\begin{bmatrix} C_{11}V_0 & C_{12}V_0|V_0| & C_{13}V_0|V_1| & C_{14}V_0|V_0|^2 & C_{15}V_0|V_1|^2 \\ C_{21}V_1 & C_{22}V_1|V_0| & C_{23}V_1|V_1| & C_{24}V_1|V_0|^2 & C_{25}V_1|V_1|^2 \end{bmatrix} \tag{3.10}$$

and the sum of its elements is equivalent to the inner product

$$\begin{bmatrix} V_0 & V_1 & V_0|V_0| & V_1|V_0| & V_0|V_1| & V_1|V_1| & V_0|V_0|^2 & V_1|V_0|^2 & V_0|V_1|^2 & V_1|V_1|^2 \end{bmatrix} \begin{bmatrix} C_{11} \\ C_{21} \\ C_{12} \\ C_{22} \\ C_{13} \\ C_{23} \\ C_{14} \\ C_{24} \\ C_{15} \\ C_{25} \end{bmatrix} \tag{3.11}$$

If the input to the amplifier is the n-sample signal [x(1) x(2) ... x(n-1) x(n)] and the corresponding output is [y(1) y(2) ... y(n-1) y(n)], then the solution to

$$\begin{bmatrix} x(2) & x(1) & x(2)|x(2)| & x(1)|x(2)| & x(2)|x(1)| & x(1)|x(1)| & x(2)|x(2)|^2 & x(1)|x(2)|^2 & x(2)|x(1)|^2 & x(1)|x(1)|^2 \\ \dots & x(2) & \dots & \dots & \dots & x(2)|x(2)| & \dots & \dots & \dots & x(2)|x(2)|^2 \\ x(n-1) & \dots & x(n-1)|x(n-1)| & \dots & \dots & \dots & x(n-1)|x(n-1)|^2 & \dots & \dots & \dots \\ x(n) & x(n-1) & x(n)|x(n)| & x(n-1)|x(n)| & x(n)|x(n-1)| & x(n-1)|x(n-1)| & x(n)|x(n)|^2 & x(n-1)|x(n)|^2 & x(n)|x(n-1)|^2 & x(n-1)|x(n-1)|^2 \end{bmatrix} \begin{bmatrix} C_{11} \\ C_{21} \\ C_{12} \\ C_{22} \\ C_{13} \\ C_{23} \\ C_{14} \\ C_{24} \\ C_{15} \\ C_{25} \end{bmatrix} = \begin{bmatrix} y(2) \\ \dots \\ y(n-1) \\ y(n) \end{bmatrix} \tag{3.12}$$

provides an estimate of the coefficient matrix.

3.1.6 Coeffcients selection and accuracy of the models

One of the most critical requirements in modeling is to model the PA accurately. It is essential to clearly evaluate the performance of the model. Therefore, model performance evaluation criteria should be adopted to choose the proper model. The most commonly used criteria are NMSE. In the following sections, the test signal for the models is the LTE signal with 8 dB PAPR and a channel of 20 MHz. The device under test (DUT) is a wideband power amplifier YSF 322+ from mini-circuits.

3.1.6.1 NMSE

NMSE refers to Normalized Mean Square Error, which is an estimator of the overall deviations between the predicted and measured values in the time domain. Therefore, it is the most straightforward approach and it is often expressed in decibels. Eqn (3.13) gives the method to calculate the NMSE of a model.

$$NMSE_{dB} = 10\log_{10}[\frac{\sum_{n=1}^{N}|y_{meas(n)} - y_{model}(n)|^2}{\sum_{n=1}^{N}|y_{meas}(n)|^2}] \tag{3.13}$$

where $y_{meas(n)}$ is the experimental output instant of the DUT and y_{model} is the output instant obtained from the model. Therefore, the accuracy of the model is inversely proportional to NMSE. In other words, the lower the NMSE is, the higher the model accuracy is. The NMSE can also represent the linearity of a PA with $y_{meas(n)}$, y_{model} being the input instant and normalized output instant of the PA, respectively. A -30 dB or less NMSE will mean that the PA has a very good linear behavior [21].

3.1.6.2 Model Selection

Figure 3.2 shows the modeling accuracy of the two models chosen for PA modeling. CTM model gives an NMSE of -19.21 dB. However, MP model gives an NMSE of -40.73dB. Hence MP model is chosen for further analysis in the report. To select the optimum set of coefficients to model the PAs, NMSE is measured for the MP model at a various number of coefficients, Figure 3.3. As can be seen, as the number of coefficients goes beyond 25 there is not much improvement in NMSE of the model as the increase in the number of coefficients. So, M=5; K=5 i.e. a set of 25 coefficients is chosen for further analysis in the report.

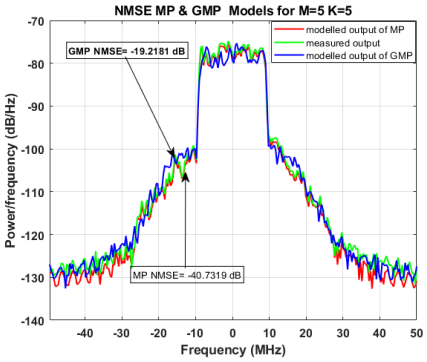

Figure 3.2: NMSE for MP and GMP for M = 5, K = 5

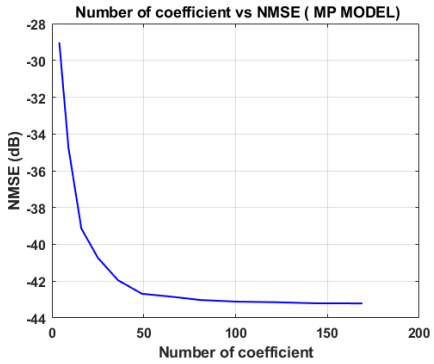

Figure 3.3: NMSE Coefficient Plot

3.1.6.3 Model Accuracy

Four PA models extracted from four physical PA's used in the 4x1 Tx antenna array measurement set up are presented here. It can be observed that all four models match to a good degree to their physical PAs. NMSE values are quite low -40dB which is a good figure of merit. Also, all PA model output characteristics match each other to good degree hence suitable to be used for our simulation setup. The four models are shown in Figure 3.4, Figure 3.5, Figure 3.6 and Figure 3.7

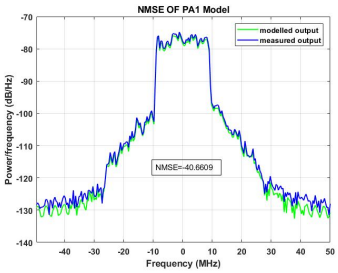

Figure 3.4: NMSE of PA 1 Model

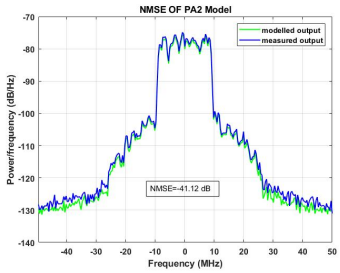

Figure 3.5: NMSE of PA 2 Model

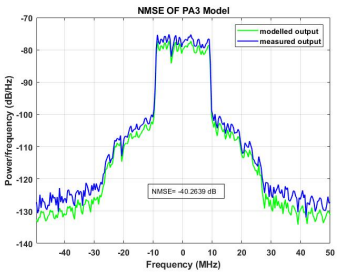

Figure 3.6: NMSE of PA 3 Model

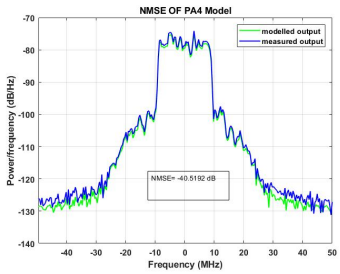

Figure 3.7: NMSE of PA 4 Model

3.2 Digital Predistortion (DPD)

Baseband digital predistortion (DPD) has become a preferred choice for the linearization of RF power amplier because of its relative simplicity and good performance. Different from feedforward and feedback techniques, the DPD technique is achieved by placing a nonlinear block, called Predistorter, just in front of the PA as shown in Figure 3.9. This predistorter produces an inverse behavior of the PA so that the final output of the PA is a linerazied output. The baseband DPD is highly popular mainly because of its flexible implimentation and good accuracy as a digital signal processing technique.

For hardware implimentation of DPD technique in wireless applications FPGA is a good choice. It affords flexible implementation, high speed processing, parallel computation and high reliability for digital signal processing applications [21].

3.2.1 Basic Principle

The basic principle of digital predistortion is to introduce a nonlinear component, called Predistorter, just before PA. The objective of this nonlinear block is to produce the nonlinear behavior which is the reverse of the PA's nonlinear behavior in both magnitude and phase, Figure 3.8 and Figure 3.10. In this way, the predistorter will counteract the nonlinearity of the PA and the final behavior will be linear, as shown in Figure 3.9.

The functioning of predistorter could also be understood in frequency domain. Since PA is a nonlinear device it generates intermodulation distortion (IMD) products. Now

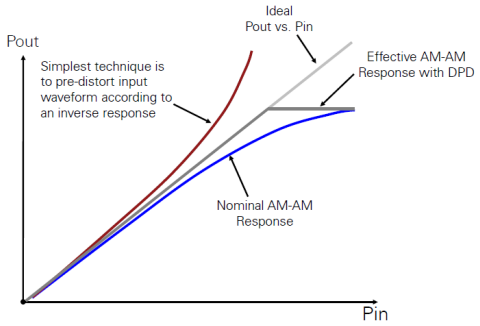

Figure 3.8: Pre-Distortion of Input Waveform

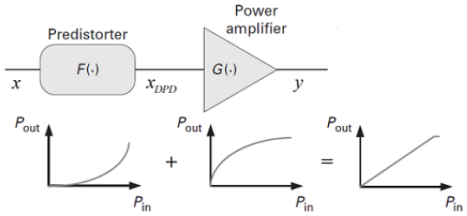

Figure 3.9: Basic Principle of Digital Pre Distortion

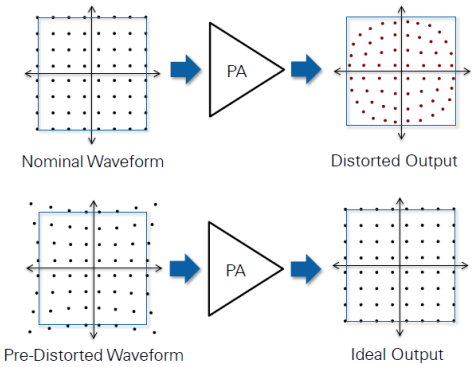

Figure 3.10: DPD applied to Digital Modulation[12]

if predistorter is also adapted to generate IMD products of equal in magnitude and 180 degree out of phase, the distortion will be cancelled, as shown in Figure 3.11 in which the downward arrow means the anti-phase [21].

In the following, the principle of DPD will be explained with mathematical equations. The predistorted signal, denoted as x_{DPD}, is

$$x_{DPD} = F(x) \tag{3.14}$$

where x is the input signal. The predistorted signal can be expressed in another form:

$$x_{DPD} = G_{DPD}.x \tag{3.15}$$

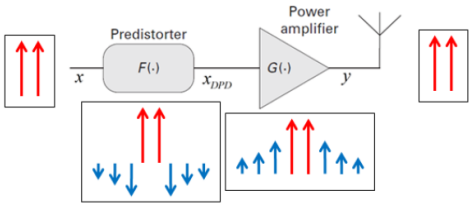

Figure 3.11: Frequency domain interpretation of Digital Predistortion

where $G_{DPD}(x)$ can be seen as the nonlinear gain of the predistorter at point x, or it is the slope of the transfer function between x_{DPD} and x. The predistored signal will be fed to the PA and the output signal will be

$$y = G(x_{DPD}) = G(F(x)) \tag{3.16}$$

which can also be expressed as

$$y = G(x_{DPD}).x_{DPD} \tag{3.17}$$

where $G(x_{DPD})$ is the nonlinear gain of the PA and also can be seen as the slope of the transfer function between y and x_{DPD}. Since the PA and the predistorter have the opposite nonlinear behavior, under the assumption that the output signal y is normalized by the power gain of the PA, we will have

$$G_{DPD} = \frac{1}{G_{PA}} \tag{3.18}$$

The gain of the entire system, consisting of both predistorter and PA, can be derived by

$$G = \frac{dy}{dx} = \frac{dy}{dx_{DPD}}.\frac{dx_{DPD}}{dx} = G_{PA}.G_{DPD} = 1 \tag{3.19}$$

Therefore, the gain of the system is 1, a normalized constant, which means that the system is linear [21].

The DPD technique is implemented in digital domain, where digital signal pro-cessing technique is applied to simplify the computation. Analog-to-digital (ADC) devices are needed to convert the analog signal into digital domain. Then a model is required to describe the predistorter and to generate the predistorted signal. The digital predistorted signal should pass through a digital-to-analog (DAC) to be converted back to analog signal. At last, the signal will be up-converted to the required frequency and is fed to the PA [21].

3.3 DPD Architecture

The basic principle of digital predistortion technique is to introduce a non-linear component which has the inverse characteristic of the PA as can be seen in open loop configuration Figure 3.12. Therefore, it is essential to derive the inverse model with the input and output data of the PA. The model inverse structure is to find an inverse function to be used as the model of predistorter. This is done by running DPD in a closed loop configuration shown in Figure 3.13 Indirect Learning Architecture is explained here.

Figure 3.12: DPD Open Loop Configuration

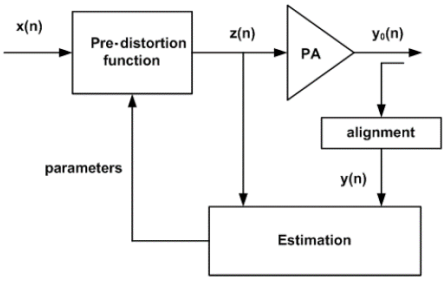

Figure 3.13: DPD Close Loop

3.3.1 Indirect Learning Architecture

Indirect learning architecture, which introduces a post predistorter, is commonly used method in the model parameters extraction for predistorter. Its basic schematic is depicted in Figure 3.14, in which $x(n)$ is the input to PD, $y(n)$ is the output from PD and also the input to PA, $z(n)$ is the normalized output from PA, is the output from the post predistorter block, the error signal e(n) is given by $e(n) = y(n) - \hat{y(n)}$. The post-inverse estimation block and the predistorter have the identical nonlinear transfer function. The post-inverse estimation block generates the parameters of PD by minimizing the error signal $e(n)$. Since that when the PA is linear, $x(n) = z(n)$ and thus $y(n) = \hat{y(n)}$. Finally, the estimated parameters are copied to the predistorter [21].

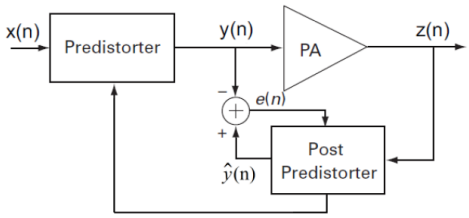

Figure 3.14: Indirect Learning Architecture

3.4 DPD Problems

Since the pre-distorter introduces the nonlinear distortion compensation which requires sampling rate of x_{DPD} to be several times higher than the sample rate associated with input signal x. This pushes the expansion in bandwidth requirement for predistorted signal x_{DPD}. This is also reflected in higher requirement on digital-to-analog converters (DACs). Thus, the DAC speed limitation will restrict the maximum bandwidth of the

input signal.

Secondly, predistorter is responsible to increase the efficency of Power Amplifiers by pushing normal PA charachterstics in high PAE zone. Thus, the primary aim is to save the energy consumption of PA. In such a scenario predistorter can not afford to loose several watts. DPD technique is found to be suitable for PAs that exceeds 10 W. The size of the hardware implimentation of the predistorter matters most for total energy consumption. Therefore, the complexity of the predistorter should not be too high in order to reduce the energy consumed in predistorter.

The value of PAPR, defined as the ratio between the peak power and the average power, becomes larger after the predistorter since the predistorter has a gain expansion. High PAPR exacerbates PA problem. Also for LTE signals PAPR is even higher (8dB - 12dB) as shown in the Figure 3.15 which means that PA's spend less time operating at their point of peak efficiency. Therefore, the input power level should back-off by more than the original PAPR from the saturation level [21].

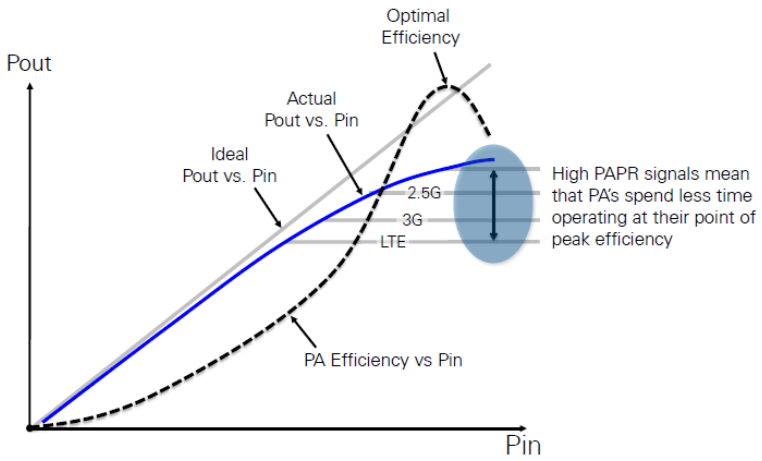

Figure 3.15: High PAPR problem for LTE signals

Chapter 4

Advanced Antenna System (AAS)

In general, an advanced or smart antenna system is a system using an antenna array together with a processor that can adjust the radiation pattern to the desired user. This system is capable of directing the maximum radiation of the array antenna pattern towards the signal of interest and at the same time, place nulls towards the signal not of interest, thereby minimizing the co-channel interference [43].

This chapter is organized into following sections: First, the used antenna in the project is shown and discussed. Later, antenna array basics and synthesis method are discussed with simulated results. In the next section, beamforming basics and digital beamforming theory with precoding are explained. In section 4.5, the requirement of coherent signal sources is discussed and validation of signal coherency for the test setup is illustrated.

Figure 4.1: PIFA Antenna

Figure 4.2: Antenna Module

4.1 Antenna in this Project

To build the measurement setup, we have used a dual band ISM band Wifi embedded PIFA antenna. The antenna element, shown in Fig. 4.1, is suitable for frequency range 2.4 to 2.49 GHz. The peak gain of the antenna is 1.5dBi at 2.44GHz. The antenna module,

shown in Fig. 4.2, is made using a semi-rigid cable to make the antenna suitable for proper RF connection.

4.2 Antenna Arrays

In many wireless applications, usually in long distance communications, high gain or directivity towards a certain direction is required. Radiation produced by the single antenna is less efficient as radiation beamwidth produced by a single antenna element is too wide for those applications. A narrow beam is needed to increase gain towards a certain direction. To achieve directional narrow beam, an antenna array is used. An array is formed using more than one radiating element and placing N spatially separated antenna in certain geometrical configuration. Proper current excitation is applied to each antenna element to form the desired beam towards the desired direction.

Array synthesis is needed to have the required beam pattern. For proper array synthesis, number of array elements , spacing between element and geometrical orientation of the array is important.

4.3 Array Synthesis

By properly synthesizing an array, several main beams can be generated using the same sets of multiple antennas. The beam can be steered so that the array produces a high gain radiation pattern towards several desired directions. Several beam specifications, i.e. sidelobe level, null constraints, etc. need to be considered in synthesizing an array to get the desired beamwidth and beam pattern. If an array is properly synthesized, we can use precoding during the signal processing to modify the phase and/or amplitude of the current excitations to control the radiation pattern. We can also modify the phase and/or amplitude electronically using phase shifters.

An antenna array synthesis consists of several steps to properly design and to meet specifications regarding beam pattern. Generally, the following steps are considered:
1. Building an array by calculating array factor, element spacing, array orientation.
2. Weighting method and weight optimization.
3. Geometry optimization in antenna arrays.

Our scope was limited to only step 1-2 without considering weight optimization technique. Since we didn't design the antenna, therefore, our scope is only limited to find the following parameter from MATLAB simulation:
1. Find optimum element spacing.
2. Find optimum scan angle.
3. Find steering vector and weight for certain direction.
4. Calculate far field distance.

4.3.1 Patch Radiation Pattern (Simulated)

The radiation pattern of the element is required for array synthesis. We designed a simulated patch considering center frequency 2.44 GHz by following the design parameter

given in [24].

Patch antenna radiates outward to the ground plane and maximum radiation occurs towards the perpendicular $(z = 0)$ direction of the antenna plane $(x = 0, y = 0)$. Considering that, the simulation results are shown only for half of the full plane (-90° to 90°). The 3D radiation pattern is shown in Fig. 4.3a and polar 2D pattern is shown in Fig. 4.3b.

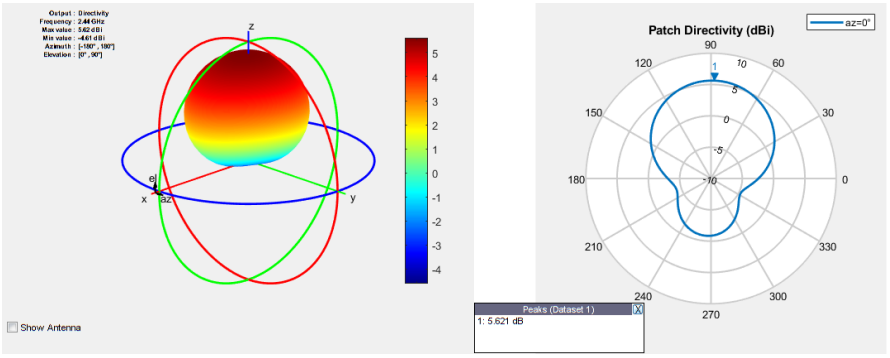

(a) 3D radiation pattern **(b)** 2D radiation pattern

Figure 4.3: Patch Antenna simulated radiation pattern

4.3.2 Uniform Linear Array

A linear array consists of N antenna elements displaced on a straight line. The array has four (N=4) element placed along the x-axis. Array elements are separated by the same distance d, leading to a total array length $D = (N - 1)d$. The center of the array in the cartesian coordinate system is the origin ($x = 0, y = 0, z = 0$). The orientation of the array is shown in Fig. 4.4a. The vector that contains the location d_n of the n^{th} antenna element is $D_n = [x_n y_n z_n]$, where $n = 1, 2, 3, 4$. The set of locations of a 4-element antenna array is $D_N = [D_1 D_2 D_3 D_4]$.

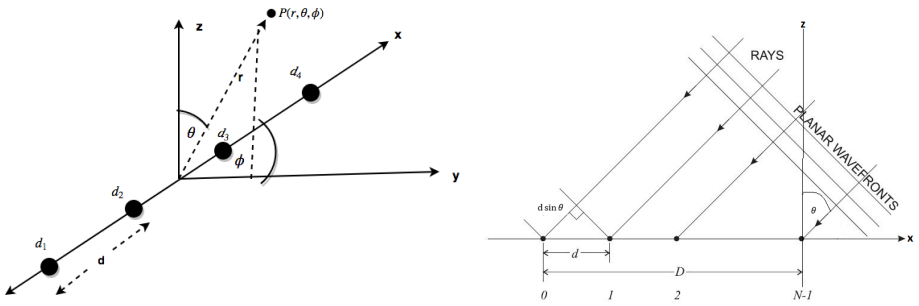

(a) Array Orientation **(b)** Array Ray Diagram[20]

Figure 4.4: Uniform Linear Array (ULA)

From Fig. 4.4b, it can be seen that element spacing between adjacent elements is equal(=d) and all excitation are identical in amplitudes. If the phase of the k^{th} element is increased by a constant progressive phase $\beta = d\sin\theta$ with respect to the (k -1)-th element, then an uniform linear array (ULA) will be formed.

4.3.3 Array Factor (AF)

In the Fig. 4.4b, it can be seen that plane waves are incident from an angle θ relative to the z-axis. The E-field of the plane wave (assumed to have a constant amplitude everywhere) can be written as [4]:

$$E(x, y, x) = e^{-jkr} \tag{4.1}$$

where, $r = \sin(\theta)\cos(\phi)x + \sin(\theta)\sin(\phi)x + cos(\theta)z$ and $k = \frac{2\pi}{\lambda}$ is the wave vector. The (z,y) coordinates of each antenna is $(0°, 0°)$. Only the x-coordinate changes for each antenna. Now assume that each element is excited with a signal of constant amplitude. Since, the transmission paths between elements are not equal, the phase shift of each element will be different. With this understanding, array factor can be defined as [20]:

$$AF = e^{-j\beta_0} + e^{-j\beta_1} + e^{-j\beta_2} + ... + e^{-j\beta_m} \tag{4.2}$$

In (4.2), phases of an incoming plane wave at the element locations i.e. $m = 0, 1, 2....m$, is β_m. In Fig. 4.4b, it can be seen that the phase of element m + 1 leads the phase of element m by $kd\sin\theta$, since the path length to element $m + 1$ is $kd\sin\theta$ metres longer than that to m. For the array geometry depicted in Fig. 4.4b, the element lies along the

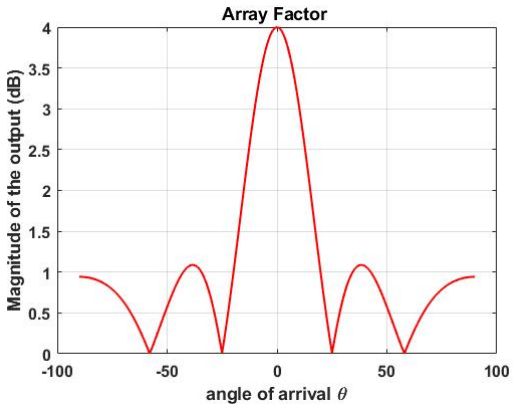

Figure 4.5: Array Factor

x-axis and centered at $x = 0$. Thus, the array factor will be according to the equation given in (4.3) and (4.4).

$$AF(\theta, \phi) = \sum_{D_{N=1}}^{D_{N=N}} e^{-jKD_N d\sin\theta} \tag{4.3}$$

$$= e^{-jKD_1 d\sin\theta} + e^{-jKD_2 d\sin\theta} + e^{-jKD_3 d\sin\theta} + e^{-jKD_4 d\sin\theta} \tag{4.4}$$

Simulation using (4.4) was done in MATLAB and result of calcualted array factor is plotted in Fig. 4.5.

4.3.4 Array Radiation Pattern (Simulated)

Calculation of the radiation pattern of antenna array is based on calculation of the total electric field intensity E_{total} at the point of observation P as given in Fig. 4.4a. E-field at a point P for a single element placed at origin is given as [33] :

$$E_n(\theta, \phi) = F(\theta, \phi) \ * \ I_n * e^{-jKD_n d \sin\theta + \delta_n} \tag{4.5}$$

Where, I_n and δ_n are the amplitude and phase excitation respectively of the n^{th} element.

The field created by a single element and Array factor is multiplied to get the total field of the array as given in 4.6. This is so-called patter multiplication rule valid for arrays of identical elements.

$$F(\theta, \phi) = E_n(\theta, \phi) * \ AF(\theta, \phi) \tag{4.6}$$

Array 3D radiation pattern and rectangular plot of array radiation pattern are shown in Fig. 4.6a and Fig. 4.6b respectively. Amplitude excitation (I_n) and phase excitation(δ_n) in (4.5) are determined by specific design of beam forming network [33].

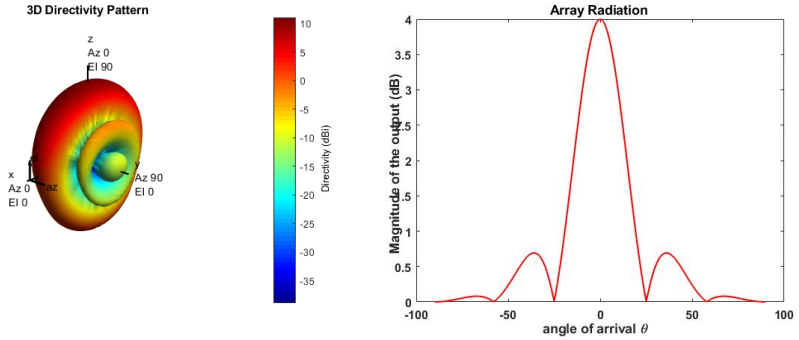

(a) 3D radiation pattern **(b)** Array pattern (Rectangular)

Figure 4.6: Array radiation pattern

4.4 Beamforming

By controlling amplitude and phase, as mentioned in section 4.3.4, the shape and direction of the signal beam from multiple antennas can be controlled. As a result, when signals of each element added, either constructively or destructively, they form the desired beam. This technique is called beamforming.

When the phase of the array is adjusted electronically, it is called analog beamforming [36]. On the other hand, when precoding is used in signal processing at baseband to form the beam without steering actual beams into the channel, it is called digital beamforming [36].

4.4.1 Digital beamforming

In digital beamforming, different signals are designed for different antenna elements of the array in a digital baseband domain using beam weighting or precoding. In precoding method, digital baseband I/Q data are weighted by adjusting their amplitudes and phases. To steer peak of the radiation pattern towards desired direction, weights for the array element are chosen properly.

4.4.2 Beamformer modelling

A simple structure to illustrate digital beamforming architecture [43] is shown in Fig. 4.7. The received signals s(t) are multiplied by a complex weight in the processor. These weighted signals are then summed to form the array output $Y(t)$ as,

$$Y(t) = \sum_{n=1}^{N} W_n^* X_n(t) \tag{4.7}$$

Where, N = number of element, $W = weightvector = [\, W_1, W_2 ..... W_N]T$ and signal induced on all elements is $X(t) = [X_1(t), ..., X_N(t)]T$

By manipulating the weight matrix W in (4.7), beam can be pointed towards any wanted direction. The general and simple beamforming scheme is beam steering; also

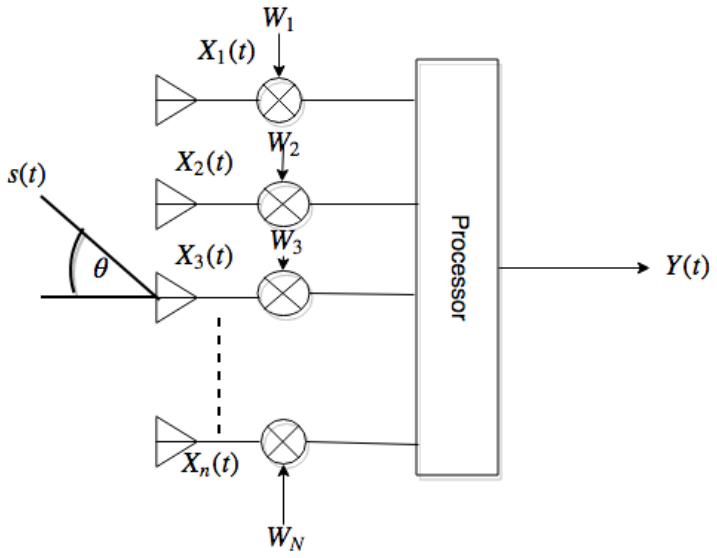

Figure 4.7: Digital Beamforming Architecture

known as conventional beamformer [43]. Keeping the amplitudes equal, the phases are selected to steer the main beam of the array in a direction θ_i.
The array weights (W) can be obtained by [43];

$$W = \frac{1}{N}[a(\theta_i)] \tag{4.8}$$

where, N = the number of element and $a(\theta_i)$ = steering vector at the direction θ_i as given in 4.9,

$$a(\theta_i) = [1, e^{-j\frac{2\pi d}{\lambda}\sin(\theta_i)}, ...e^{-j(N-1)\frac{2\pi d}{\lambda}\sin(\theta_i)}]^T \tag{4.9}$$

We can write the array factor using the steering vector as: $AF(\theta, \phi) = W^T a(\theta_i)$. Proper weight calculation is needed for precoding the IQ baseband signals to steer the beam in certain direction.

4.4.3 Weight and Steering Vector

For correct weight and steering vector calculation, we have to optimize two parameters of the array. One is a proper element spacing and the other one is scan angle or look angle.

4.4.3.1 Grating Lobes

If the inter-element spacing of a Linear array exceeds half a wavelength, grating lobes from the invisible region start to appear in the visible region $[[-90°90°]$. To avoid grating lobes, inter-element spacing should be chosen as $d < \frac{\lambda}{2}$ [36]. It can also be done by restricting scan angle or decreasing the element spacing. The maximum scan range $|\theta_0|$ for a given element of distance d is defined in the grating lobe criteria [36] as,

$$\frac{d}{\lambda} < \frac{1}{1 + \sin|\theta_o|} \tag{4.10}$$

In general, the cellular network consists of three sectors per cell and provide $120°$ coverage per sector [30]. One sector corresponds to a radiation pattern of a single conventional antenna. The maximum horizontal azimuth beam pattern that covers the sector is about $+/-65°$ HPBW (Half Power beam width) [30]. Thus, the primary scan angle is selected as $\theta_0 = 60°$ and the element spacing using (4.10) is found as $d = 0.5359\lambda$. However,

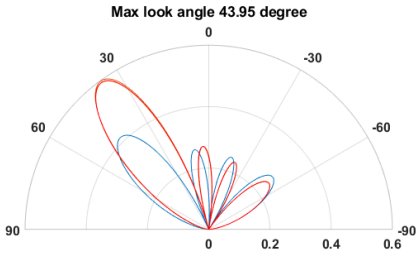

Figure 4.8: Scan Angle Optimization

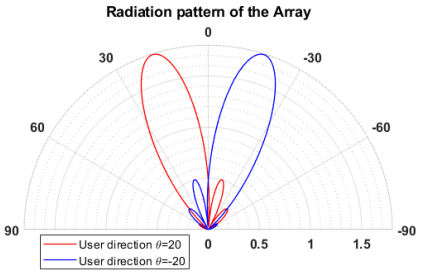

Figure 4.9: Beam steering

the bandwidth of the main beam needs to be considered to find out maximum scan angle. The array factor (AF) discussed in section 4.3.3 is used for the calculation of revised scan angle by following the below steps:
(i) Taking initial scan angle $\theta = 60°$, the beam width is calculated.

(ii) Based on the beam width, new scan angle is calculated using:
$\theta_{new} = \theta_{old} - (\frac{beamwidth}{2})$
(iii) From the new scan angle, the element spacing is calculated using (4.10). Using the iterative loop as shown in Fig. 4.8, revised maximum scan angle is found approximately as $44°$. The element spacing considering the new scan angle is $d = 0.5901\lambda$. We can now steer the beam in any direction by calculating weight using (4.8) and (4.9). Beam steering towards different direction is shown in Fig. 4.9.

4.4.3.2 Far Field Distance

Antenna Far field is the region where radiation field decay as $\frac{1}{r}$. In far field region, the radiation pattern is independent of r, where r is the distance from the antenna. From the calculated element spacing, the total maximum aperture D of the array is found and far field is calculated using the far field criteria, $r < \frac{2D^2}{\lambda}$. The far field is found as approximately 1m.

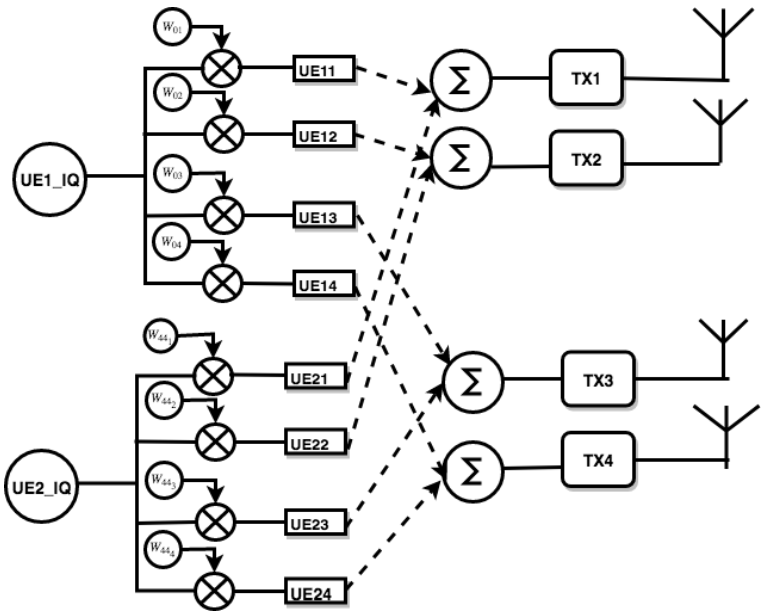

Figure 4.10: Element space beamforming

4.4.4 Precoding

Two different I/Q signals (100 Msample, 20MHz LTE) were generated for two user directions. The weight matrix, for two different directions i.e $0°and\ 44°$, were calculated by following the method discussed in the section 4.4.3 and 4.4.2. Precoding is done by processing the signal according to the block diagram shown in the Fig. 4.10. This is known as element–space beamforming [44]. The two data signals for two users in two different directions are processed using a weight vector to form the beam towards the desired di-

rection. Finally, we got the four precoded signals suitable for transmission through the antenna array for beamforming application.

4.5 Phase Coherent Signal Generation

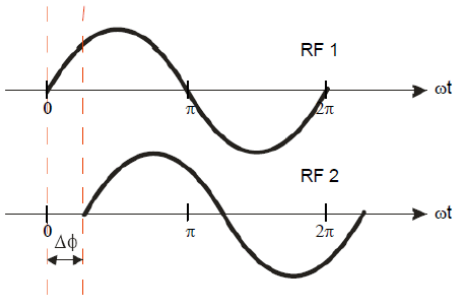

Figure 4.11: Phase coherent signals [35]

The application of cellular communication's beamforming sectors or the testing of multi-antenna systems such as phased array or beamforming antennas requires a system capable of providing multiple signals with constant phase relationships between them [35]. If the relative phase $\Delta\phi$ between the two signals given in Fig. 4.11 stays constant over time, signals are phase coherent . The coherent test signals should have a specific relative phase difference between them. Phase stable and coherent signals can be achieved using a common synthesizer signal (local oscillator, LO) for all signal generators [35].

4.5.1 Methods to stabilize the relative phase of four RF carriers

In our test setup, there are four independent signal generator sources. All can use an external reference frequency signal from an external source. Thus, local oscillator (LO) signal of one synthesizer was used in all other three signal generators to get the phase stability. We manually shared one local oscillator to all signal generator as shown in Fig. 4.12.

Using Digital Oscilloscope, phase coherency and relative phase stability over time were checked among the signals of the generators. A snap from the oscilloscope is given in Fig. 4.13.

4.5.2 RF phase control

Baseband signal is upconverted to RF by the I/Q modulator in a signal generator. The upconversion is done using Local oscillator signal from synthesizer. Phase of the signal can be controlled by introducing a phase offset to the digital baseband signal. Also, Phase can be controlled by adjusting the phase of the LO signal [35]. Phase adjustment of the RF signal can be made using,

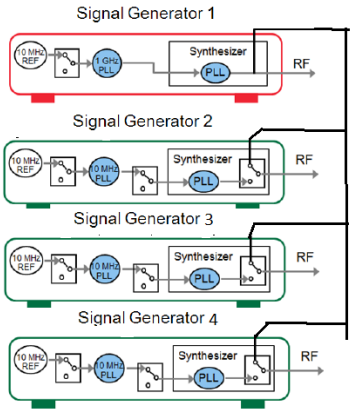

Figure 4.12: LO sharing [35]

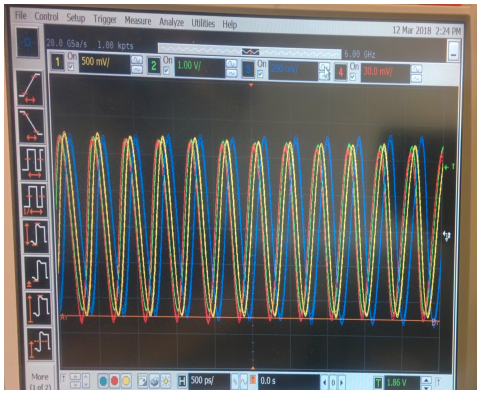

Figure 4.13: Coherent signal in digital oscilloscope

(1) Via the digital baseband by applying a phase offset to the I/Q signal
(2) Via the synthesizer by applying a phase offset to the LO signal.
Since, all signal generators are coupled via a common LO signal in the setup, setting the relative phase or each RF phase independently, can no longer be possible via the synthesizers. Thus, only phase control can be done in the digital baseband of a VSG [35]. The relative phase between carriers can be adjusted using phase offset in digital baseband.

4.5.3 Phase relationship between IQ signals

I/Q data show the changes in magnitude (or amplitude) and phase of a sine wave. The equation representing a sine wave is $A_c \cos(2\pi ft + \phi)$, where, A_c is the amplitude, f is the frequency and ϕ is the phase of the sine wave.

A sine wave instantaneous state can be represented by a vector in the complex plane using amplitude and phase coordinates as shown in Fig. 4.14. Sine wave in Fig. 4.15 is taken as a reference sine wave with frequency 1Hz and amplitude 1. The reference sine wave is modulated with cartesian IQ value:$0.354 + 0.354j$

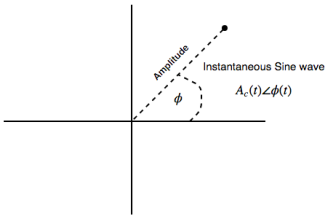

Figure 4.14: Polar represtation of sine wave

The modulated wave is shown in Fig. 4.16. If the modulated sine wave is plotted with keeping unmodulated sine wave as a reference, then the resultant plot is the Fig. 4.17.Any phase rotation around the origin indicates a frequency difference between the reference sine wave and the sine wave being plotted.

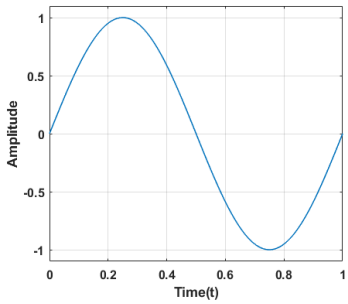

Figure 4.15: Unmodulated sine wave

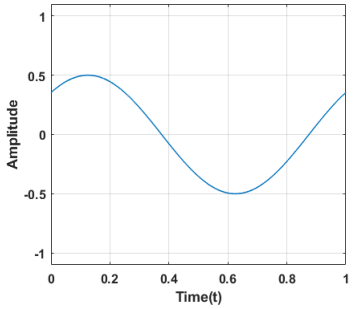

Figure 4.16: Modulated sine wave

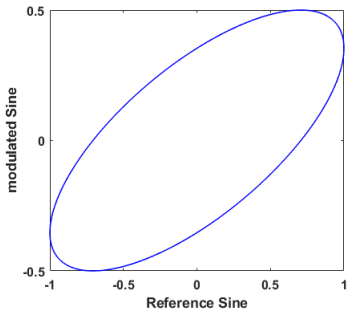

Figure 4.17: Modulated sine wave vs Reference sine wave

4.5.4 Simulated response vs measured response of RF phase control

Digital Oscilloscope has a math XY function which can be used to see the same outcome as in Fig. 4.17. We used one LTE 20MHz IQ data to transmit through the three signal generators. For the first TX branch, only the IQ data, without any phase adjustment, was transmitted. In this case, the signal from PA output is directly fed to the first channel of the Digital oscilloscope without using antenna transmission. The reason is to take the signal only as a reference signal (X-axis in digital oscilloscope MATH function).

The same IQ data were transmitted through the second signal generator and through the antenna. For the third generator, phase adjustment is added to the same IQ data and transmitted through the antenna. IQ phase of the third signal was adjusted to $60°$. Thus, the transmitted signal from the two antennae is combined over the air. The receiving antenna placed in the far field of the array and connected to the second channel of the digital oscilloscope (Y-axis in digital oscilloscope MATH function).

The simulation also performed in similar fashion as the measures described above. The simulated response and measured response can be observed in Fig. 4.18a and Fig. 4.18b respectively.

It is observed that IQ phase change of one transmitted signal was reflected in the

received signal phase because the rotation of the ellipse-like plot was observed. Both simulation and measured response in Fig. 4.18 shows the same response as the ellipse orientation is same.

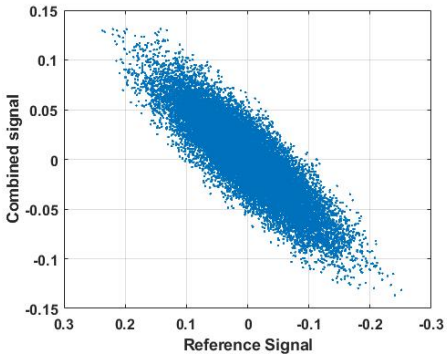

(a) Simulated response

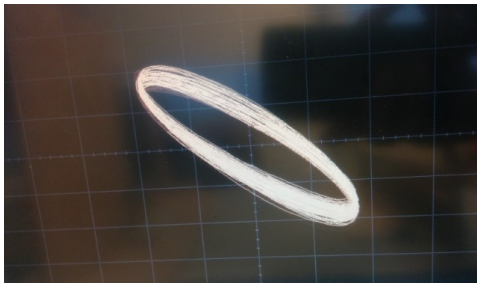

(b) Measured response

Figure 4.18: Simulated Vs measured response

Thus, it is confirmed that IQ phase adjustment works for the setup. It is required to verify that the text setup is suitable for Digital beamforming application.

Chapter 5

Crosstalk and Mismatch in Multiple Antenna System

In this chapter, firstly, sources of crosstalk are discussed. Thereafter, different crosstalk scenarios with system model are explained. Later, mutual coupling of antenna arrays is discussed with coupling measurement results. Also, the procedure of scattering parameter extraction for all antenna elements of the array is illustrated in the next section. In the following section, post PA crosstalk is focused. The impact of post-PA crosstalk on PA output signal is investigated with over the air measurement. Finally, the impact of crosstalk on DPD performance is discussed.

5.1 Sources and Impact of Crosstalk in Multi-antenna Transmitters

In general, transmitters suffer from several kinds of imperfections, e.g. gain and phase imbalance, mixer leakage. To employ several transmit path in the multi-antenna system, complexity and feasibility of analog and digital hardware design is a major concern. In designing analog hardware using large antenna array, bulky and expensive component, i.e. Isolators between PA and antenna are avoided [17]. Moreover, the ever decreasing size of the integrated circuits (ICs), on which MIMO transmitters are implemented, exacerbate the crosstalk problem. This is due to the fact that all signals in different paths, use the same operating frequency and have equal transmission power [7]. As crosstalk effect grows significantly, it leads to the generation of more nonlinearities and degrades the performance of the MIMO transmitters.

5.2 Multi-Antenna RF Transmitter system Models considering crosstalk

Along with the nonlinear distortion caused by the PA, multi-antenna transmitter suffers from distortion due to the crosstalk effect. Crosstalk can be categorized into three major types which are following:

- Crosstalk originated before PA at the transmitter RF front-end and nonlinear in nature [16].
- Crosstalk after the PA which is purely additive (Linear) [16].
- Antenna crosstalk and mismatch due to coupling [17].

When designing a multi-antenna system, these crosstalk effects need to be considered in defining the system model. Thus, understanding these system models is necessary to further investigate the problem. All different crosstalk can be defined by the independent system model [17]. In the following sections, these system models are illustrated with individual system model.

5.2.1 Systems Without Crosstalk

If there is good isolation among the branches, between PAs and antennas, distortion is only because of PA nonlinearity. This scenario can be modelled [17] using equation(5.1) and is shown in Fig. 5.1. The output of the k^{th} transmit branch depends only on the input of that branch, i.e.

$$Y_{1k} = f_k(X_{1k}) \tag{5.1}$$

where $f_k(.)$ is the nonlinear function of the PA , X_{1k} is the input signal of the K^{th} branch. These notations are same for all model that are described in later sections.

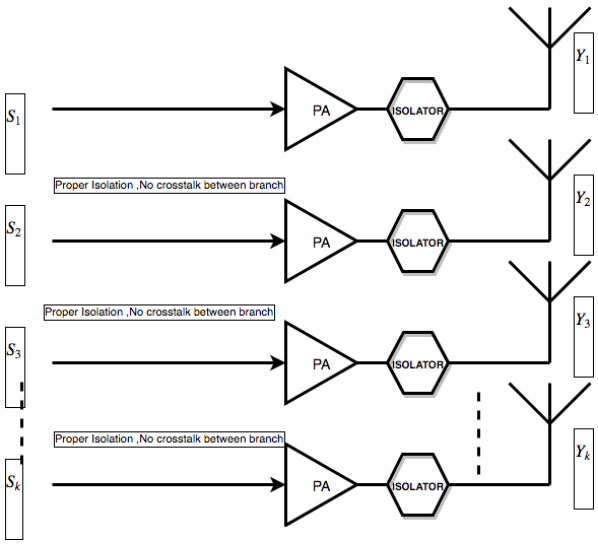

Figure 5.1: Multi-antenna transmitter system model without crosstalk

5.2.2 Crosstalk Before PA

This type of crosstalk occurs mainly due to the leakage of RF signal through the common local oscillator (LO) and interference in the chipset between different transmit path as

a result of EM coupling [2]. Furthermore, any crosstalk before PA is amplified by the power amplifier which is a nonlinear device. Thus, this type of crosstalk is called as non-linear crosstalk. The nonlinear crosstalk and the PA nonlinear response should be jointly compensated by a multi-antenna predistorter to get a reliable system performance [16]. As shown in Fig. 5.2, we can consider any transmit branch k^{th}, in which input to the PA is the linear addition of all other interfering signals, i.e PA input= $u_k(X_{11}, X_{12}, X_{13}, ...X_{1k})$ and $u_k(.)$ is the linear function of all interfering signals. Then, the output from the branch can be modelled using (5.2).

$$Y_{1k} = f_k(u_k(X_{11}, X_{12}, X_13, \dots X_{1k})) \tag{5.2}$$

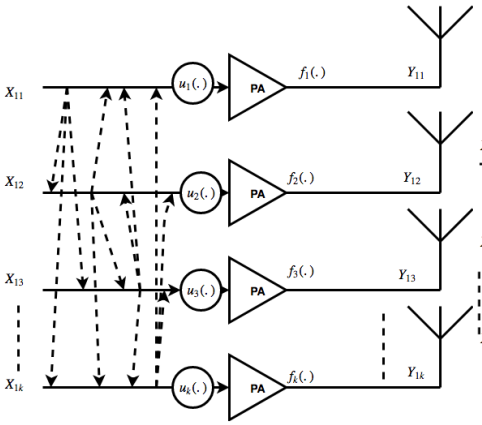

Figure 5.2: Crosstalk before PA

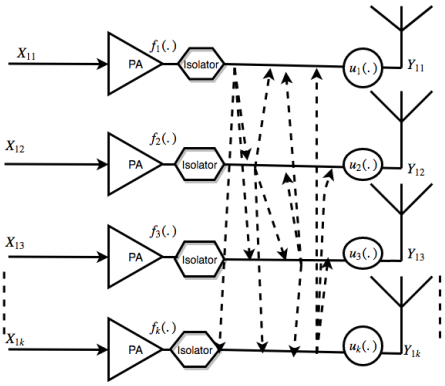

Figure 5.3: Antenna crosstalk after PA (Linear)

5.2.3 Linear (Antenna) Crosstalk after PA

Crosstalk after the PA originates due to the coupling of the transmitted signals from one antenna element to another antenna element, considering that isolators are used between PA and antenna [17]. As this crosstalk does not pass through any nonlinear device, it is considered as linear crosstalk. The effect of linear crosstalk can be compensated or mitigated at the receiver side [7, 31].

The system model is shown in Fig. 5.3 where output in (5.3) from the k^{th} transmit branch is the linear function of all other interfering signals after the PA.

$$Y_{1k} = u_k(f_1(X_{11}), f_2(X_{12}), f_3(X_{13})..f_k(X_{1k})) \tag{5.3}$$

5.2.4 Antenna Crosstalk and Mismatch

If no isolators are used between PA and closely packed antenna in an integrated multi-antenna transmitters, the crosstalk and mismatch discussed in section 5.2.3 mixes with the PA output. This phenomenon is described and modelled using a k-port network [6] as shown in Fig. 5.4. The output wave of each PA device, as shown in Fig. 5.4, can be

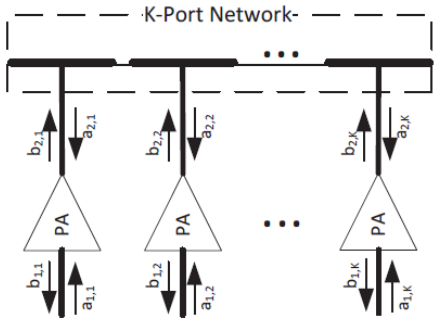

Figure 5.4: Antenna array with several RF PAs [6]

written as:

$$a_{2,i} = \sum_{k=1}^{K} S_{i,k} b_{2,k} \tag{5.4}$$

Where, $a_{2,i}$ is the reflected wave at the output of the i^{th} device and $b_{2,k}$ is the incident wave at the output of the k^{th} device.

Analyzing (5.4), it can be noted that output wave from the i^{th} device are correlated with the all waves coupled from other devices. Generally, this scenario is common in phased arrays and beam-steering applications. As a result, each PA operates under varying load. The equivalent load in (5.5) is dependent on the output of each PA and the mutual coupling of the antennas [6].

$$C_{i,k} = \frac{b_{2,k}}{b_{2,i}} \tag{5.5}$$

Each PA is excited by two signals. The output of the PA is excited by one signal and the input is excited by other. This output excitation is called load modulation which is shown in Fig. 5.5.

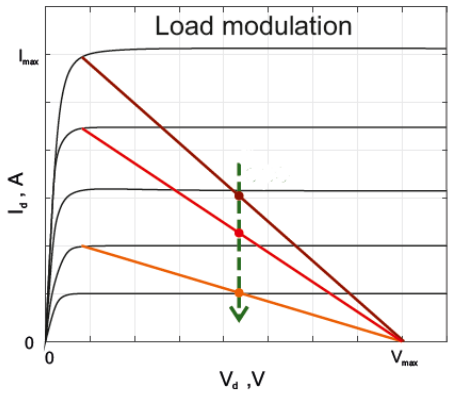

Figure 5.5: Load modulation [34]

The load line [34] in Fig. 5.5 is drawn using equation(5.6), in which the output voltage,V_d and current swing I_d are set by load termiantion R_L and DC bias voltage $V_{D,bias}$. If the output voltage or load termination changes, the load line characteristics changes accordingly.

$$V_d = V_{D,bias} - I_d R_L \tag{5.6}$$

The linearity of PA is impacted by this load modulation. The impact on the linerity of PA for this excitation has been presented in some previous work [3, 6]. In [26, 37], this problem has been addressed and solutions has been proposed. In [6], it has been stated that a global approach to compensate the PA in this configuration would be to consider the input excitation for each device and create a multiple input digital predistorter (DPD). In [17] , dual input PA model has been proposed. The dual input PA model is not further discussed in this thesis.

To understand the dual excitation behavior of the RF PA , Mutual antenna coupling in antenna arrays need to be investigated.

5.3 Mutual Coupling in Antenna Array

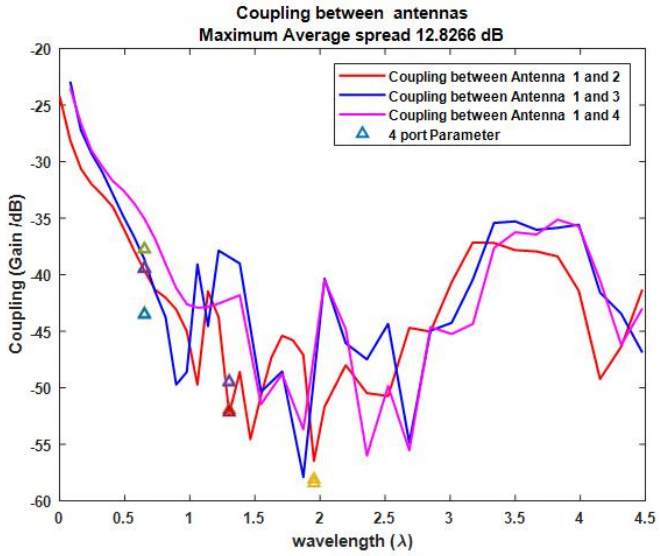

Figure 5.6: Coupling vs Distance

Mutual coupling between antenna is an electromagnetic phenomenon. It occurs due to the change of the electric current distribution on the antenna. When an object or another antenna is brought in the near field of a given radiator antenna, the changes [19] are as following;

- Radiator antenna can absorb a fraction of the radiated power by other antenna and input impedance is modified.
- Radiation pattern are modified.

There have been many methods proposed to study the effect of mutual coupling in array antennas. It is getting more significant because of the ever-decreasing size of radio transceivers and small-size antenna arrays. One of the best ways to study the mutual coupling on antenna arrays is from the corresponding S-parameters between the elements of the array. Amount of coupling can be realized using S-parameters which is illustrated in (5.4) and (5.5).

To understand the impact of mutual coupling, S-parameters were measured using a vector network analyzer between two antenna elements by varying the distance between elements. Several combinations of two antenna elements were tested using two-port VNA measurements. The plot in Fig. 5.6 clearly depicts the coupling phenomena between antenna elements. The more closely the element to each other, the coupling amount increases, which is visible in Fig. 5.6. Also, the similar trend of coupling found in different combination of elements, which is expected as antenna elements are same ISM band with same properties.

Coupling values of the 4X1 uniform linear array were measured via 4-port VNA measurement. These S-parameter values are also shown in Fig. 5.6 which shows that coupling depends on various properties of the array. Coupling depends on distance between antenna, antenna array structure e.g. linear, planar and frequency or wavelength of the array design.

5.3.1 Scattering Parameters Extraction

To model the crosstalk of the array, measurements of the antenna array scattering characteristics (S-parameters) are required. Since the array is a 4X1 linear array as shown in Fig. 5.7, 4-port measurement is the simplest way to extract the coupling values between the array element. 4-port measurement setup is shown in Fig. 5.8. We used 4-port vector network analyzer to extract the S-parameter values of the array.

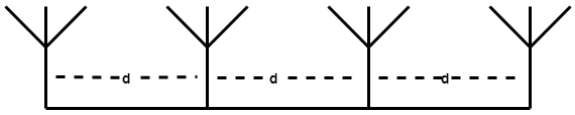

Figure 5.7: 4X1 Uniform Linear array

At first, scattering parameters were extracted for the array element spacing $d = 0.59\lambda$, which is the element spacing of the array for 2.44 GHz carrier frequency. S-parameter data from VNA was processed using MATLAB. The gain is plotted using the amplitude of the corresponding S-parameter and phase is plotted using the angle of the s-parameter data.

Phase and Gain information of all S-parameters of the first antenna element of the array are plotted in Fig. 5.9 for the frequency range of 2 GHz-3 GHz. A similar plot is shown in Fig. 5.10 for the fourth antenna element.

The Fig. 5.9 and Fig. 5.10 show that the s-parameter characteristics or the coupling nature of antenna element 1 and 4 are approximately similar. We can investigate the coupling values in Table 5.1 for the only 2.44GHz. The table shows that S12 and S43 values are almost same. A similar observation can be seen from the value of S13 and S42.

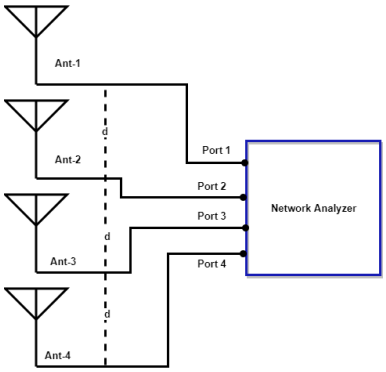

Figure 5.8: Scattering parameter extraction setup

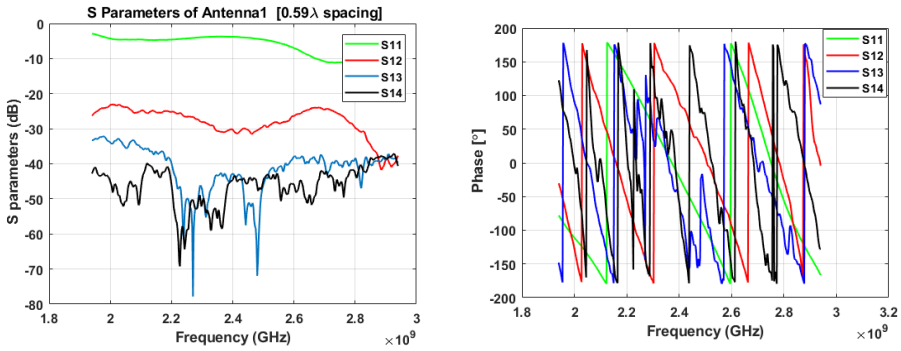

(a) S-parameters(Gain) **(b)** S-parameters(Phase)

Figure 5.9: S-parameters of Antenna element 1

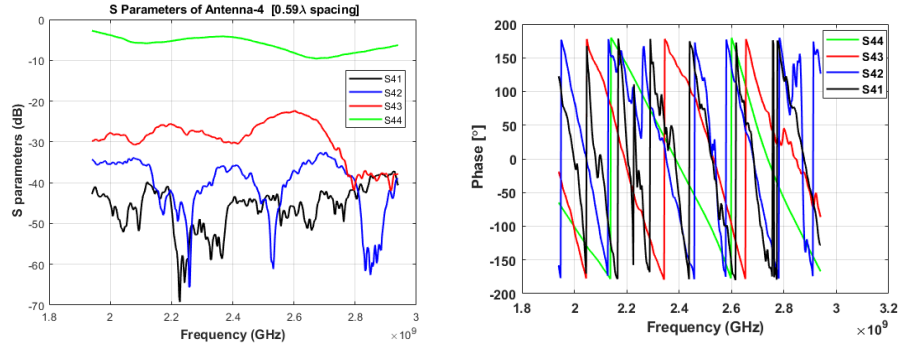

(a) S-parameters(Gain) **(b)** S-parameters(Phase)

Figure 5.10: S-parameters of Antenna element 4

Moreover, Phase and Gain information of all S-parameters for the second and third

Ant-1	Value(dB)	Ant-2	Value(dB)	Ant-3	Value(dB)	Ant-4	Value(dB)
S11	-4	S21	-30	S31	-39.78	S41	-45
S12	-29	S22	-5.37	S32	-27.32	S42	-38.63
S13	-38.8	S23	-27.32	S33	-4.36	S43	-28.5
S14	-44.96	S24	-38.62	S34	-28.9	S44	-4.85

Table 5.1: Antenna array S-paramters for element spacing=0.59λ

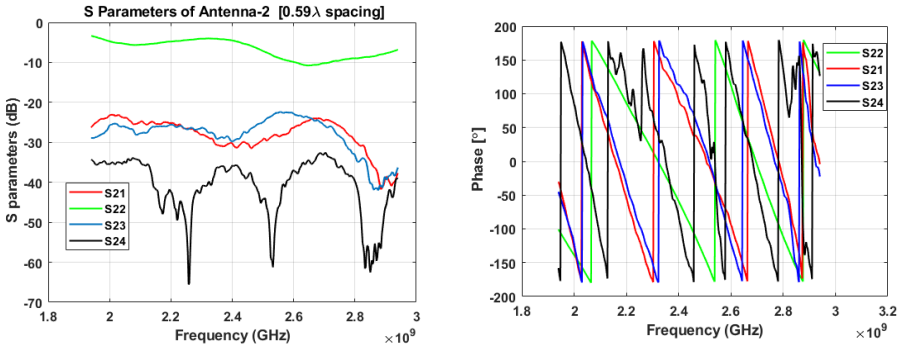

(a) S-parameters(Gain) **(b)** S-parameters(Phase)

Figure 5.11: S-parameters of Antenna 2

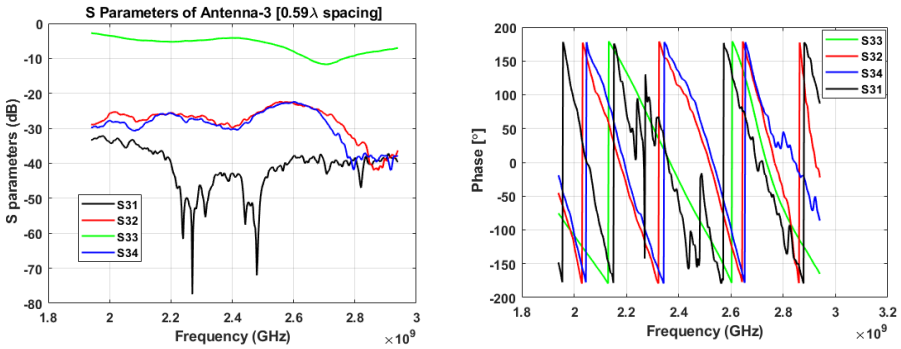

(a) S-parameters(Gain) **(b)** S-parameters(Phase)

Figure 5.12: S-parameters of Antenna 3

element of the array are plotted in Fig. 5.11 and Fig. 5.12 respectively. The Fig. 5.11 and Fig. 5.12 show that the s-parameter characteristic antenna element 2 and 3 are approximately similar. This also reflects in Table 5.1 where S24 and S31 values are almost same. A similar observation can be seen from the value of S21 and S34.

The similarities between s-parameters of antenna elements indicate the nature and trend of coupling in an antenna array. The reason for the similarities is that the antenna element position of 1 and 2 is identical with respect to the array geometry. This is also

true for element 2 and 3. If any two or more element position is identical with respect to the array geometry, the coupling or the s-parameter values are expected to be similar.

The final experiment on S-parameter characteristics was done by varying the antenna element spacing of the array. This was done to see how the element spacing impacts the coupling. The results are given in Table 5.1. Only the maximum coupling values of element spacing 0.59λ,0.41λ and 0.28λ are tabulated in Table 5.2 respectively.

Element Spacing	0.59λ	0.41λ	0.28λ
Ant1	-29.9	-23.6	-29.9
Ant2	-27.32	-22.8	-27.32
Ant3	-27.32	-22.8	-27.32
Ant4	-28.49	-23.6	-28.49

Table 5.2: Copupling vs different element spacing

The important observation is that coupling values for 0.59λ and 0.28λ are approximately same, though the letter spacing is too close to the element. This is due to the constructive and destructive nature of the waves coupled. For 0.41λ spacing, the values of s-parameter is higher than the other two cases. Element spacing doesn't define the coupling between the elements of the array. The nature and the phase of the wave define the amount of coupling between the elements of an antenna array.

The results and observation found in this section are important to understand the crosstalk or the coupling nature for an antenna array. Moreover, the S-parameter values and other coupling parameter discussed in this section will be used for simulation and modelling of crosstalk.

5.4 Modelling Post-PA crosstalk

Post-PA crosstalk combines both linear crosstalk (section 5.2.3) and Antenna crosstalk and mismatch (section 5.2.4). The system model is shown in Fig. 5.13a.

To compensate the post-PA crosstalk due to antenna mismatch and coupling, a different approach is proposed in this thesis compared to existing dual input PA model discussed in section 5.2.4. The general overview of the system model is given in Fig. 5.13b.

Fig. 5.13b gives the primary overview of the proposed approach where the s-parameter block contains all s-parameter of the array. The general idea is that, for DPD coefficient calculation and adaptation, not only PA output signal will be considered but also signals coupled from other branches of the multi-antenna transmitters will be considered. This proposed approach will be discussed in details in chapter 6.

5.5 Crosstalk Distortion analysis

The impact of post-PA crosstalk on the PA output signal need to analyzed to detect the scope of overall system performance improvement. In this section, we will analyze the distortion of the PA output signal due to crosstalk between branches and coupling between antennas. A good way to calculate the contribution of crosstalk on signal distortion is to

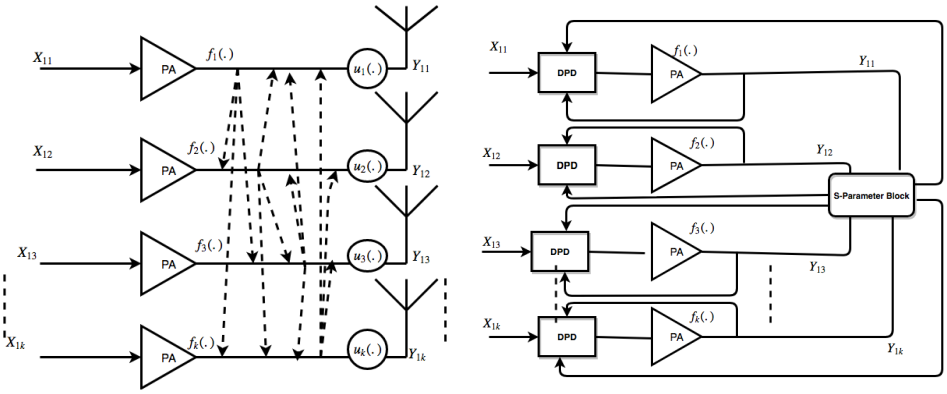

(a) Post PA crosstalk (without isolators) **(b)** System model of proposed approach

Figure 5.13: Crosstalk modelling

calculate the adjacent channel leakage ratio (ACLR) [9]. ACLR/ACPR of the PA output signal was measured for different crosstalk between the branch or coupling between antennas. Impact of post-PA crosstalk on PA output signal was analyzed for two different measurements. These measurements were done without any DPD running.

5.5.1 ACLR : directional coupler measurement

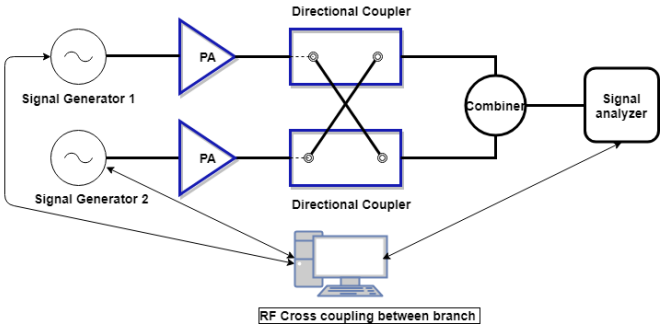

Figure 5.14: Measurement setup of coupling test (2-TX branch)

In the measurement setup shown in Fig. 5.14, signals from two PA are combined using a combiner. Directional couplers are utilized to cross coupling the signal between the branch to introduce crosstalk. The amount of crosstalk from one branch to another branch was varied using different couplers or adding attenuators to the signal path. Both the signal before combiner and signal after combiner was captured simultaneously by the signal analyzer using an RF switch. Two different IQ data were used for two branches.

The Fig. 5.15a shows the spectrum of the PA output signal of one branch. The Fig. 5.15b shows the spectrum of combined signal for varying amount of cross-coupling between two branches.

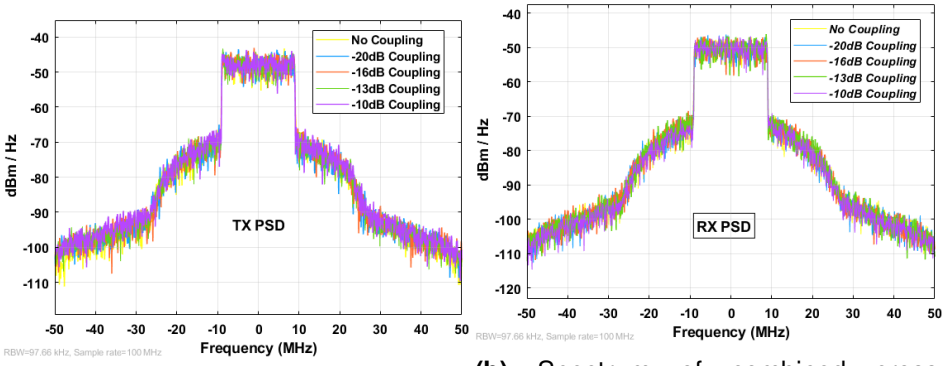

(a) Spectrum of PA output (TX)

(b) Spectrum of combined cross-coupled signal

Figure 5.15: Power Spectral density

By observing the Power spectral density of both signals in Fig. 5.15, it is noted that there is no change of ACLR level at all for any level of coupling introduced between the branches. The same observation is also found in some previous work [9, 18].

5.5.2 Over the AIR measurement using Antenna array

In this section , a brief overview of the measurement setup will be given .The complete measurement setup is shown in Fig. 5.17.

The measurement setup consists of 4 PAs, 4 antennae (TX1-TX4) for the linear array at the transmitter side, 2 antennas (UE1, UE2) as receivers or users, signal analyzer, signal generator, DC power source, RF switch and a digital oscilloscope. The antenna slider, shown in Fig. 5.16, was designed using a free CAD design tool. Then the 3D model was printed using a 3D printer. The antenna slider was needed to slide the array element properly. The weighted (precoded) signals were fetched to the respective signal generator using MATLAB. Directional couplers were used between every PA and antenna to capture the PA output signals. The Receivers were placed at a far field distance. UE2 in the picture was ignored. All four PA output signals and received signal from UE1 were captured using the RF switch and signal analyzer.

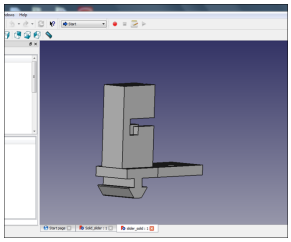

Figure 5.16: 3D design of Antenna slider

To introduce different crosstalk scenario, the coupling between the elements of the array was varied by changing the element spacing mentioned in Table 5.3.

It can be seen in Fig. 5.17 that, UE1 is placed 1m away from the center of the array at symmetry plane to the array. The placement of UE1 is approximately at 0° scan angle

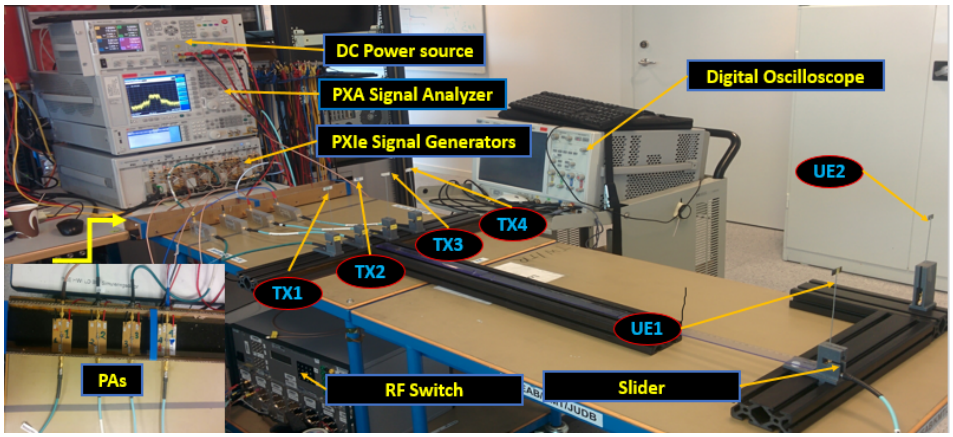

Figure 5.17: Complete measurement setup test bench

direction.

The received signal will be the result of the beamformed signal of the four transmitted signals, including channel effects as well as the effect of the receiver antenna. The nonlinear distortion observed at the receiver is independent of the receiver location. So the measurement results are presented for only one position. In Fig. 5.18a, the power spectral density of UE1 is plotted for different coupling scenario. Among four branches, the only signal from the 2nd branch was captured to show the PA output signal power spectral density shown in Fig. 5.18b.

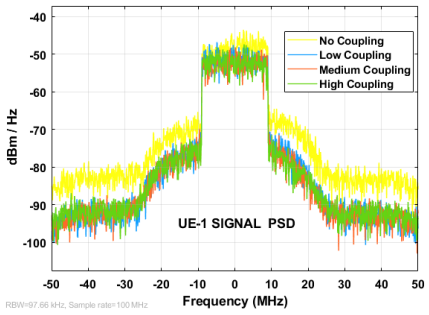

(a) UE-1 Power spectral density

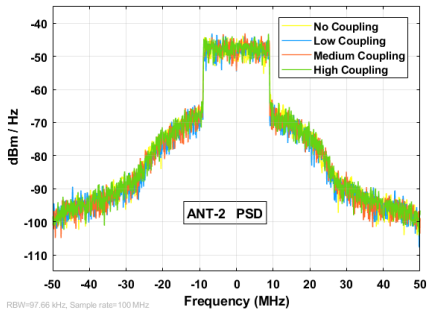

(b) PA-2 Power spectral density

Figure 5.18: Power Spectral density

It can be seen in Fig. 5.18a that, for the different coupling scenario mentioned in Table 5.3,there is no noticeable change in ACLR level of the user signal. That is also true for PA output signal as shown in Fig. 5.18b. Also, We have seen similar observation in section 5.5.1.

The measurement results discussed in section 5.5.1 and 5.5.2 is crucial for post-PA crosstalk modelling. It is found that post-PA crosstalk without any DPD doesn't impact the level of ACLR in transmitted signal.

Coupling scenario	element spacing
No	signle transmitter active
Low	0.59λ
Medium	0.41λ
High	0.28λ

Table 5.3: Copupling scenario

5.5.3 Impact of crosstalk on DPD performance

Without DPD, it is not possible to identify which part of the spectral regrowth is due to the crosstalk or due to the non-linearities of the PA. Thus, MATLAB simulation was performed in SIMULINK to see the impact of post-PA crosstalk on DPD performance. Also, our primary approach for post-PA crosstalk modelling is discussed in this section.

The primary block diagram of the method developed in chapter 6 is shown in Fig. 5.19. However, the DPD used in this block diagram is conventional DPD with no crosstalk cancelling technique.

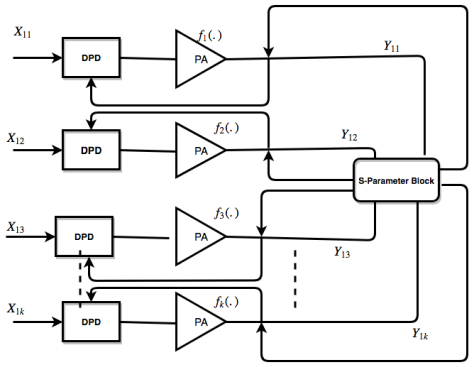

Figure 5.19: Simulation model using conventional DPD

In the simulation, behavioural models of PA from chapter 2 and extracted S-parameters of the array in section 5.3.1 were used. To emulate crosstalk, S-parameter block calculates the combined crosstalk effect on different transmit branch and fetch to the PA output of that branch. Thus, the block diagram with s-parameters of all antenna elements can create the crosstalk environment in the simulation. The output from S-parameter block in Fig. 5.19 is the combined effect of coupling from the interfering branches. This combined coupling effect and PA-output signal are again combined to fetch to DPD block.

The simulation was done in two steps. In the first step, conventional DPD was used to see the impact on the linearized output spectrum without any crosstalk without fetching the output from the S-parameter block. In the second step, the output from the S-parameter block was fetched to see the DPD performance with crosstalk environment. Four preceded signals are used for all simulations and measurements. Only the simulation result for one transmit branch is shown in Fig. 5.20.

In Fig. 5.20, it can be seen that the spectrum resulting from the use of the DPD and

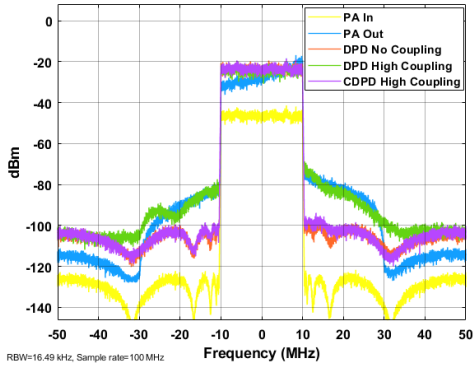

Figure 5.20: Simulation using conventional DPD

the spectrum resulting from the DPD with crosstalk are diverging. When the coupling increases ACLR worsens in DPD with crosstalk as expected , which confirms that the output signal of the PA is distorted due to the effect of crosstalk. So,the spectral regrowth will correspond to the contribution of crosstalk distortion. Under crosstalk condition, DPD ability to linearize PA becomes limited. If the DPD can't linearise the PA enough in order to reduce the distortion due to classic non-linearities of the PA below the level of distortion resulting from the crosstalk contribution, the PSD in the adjacent channel will correspond to the contribution to distortion from the non-linearities of the PA. However, if the DPD linearise the PA enough , the spectral regrowth will correspond to the contribution of crosstalk distortion. In our case, the DPD is thus not good enough.

The 3GPP standard requirements for the ACLR is at least -45dB [9]. That means that above this limit (ACLR $> -45dB$) the requirements are not fulfilled and the crosstalk effect cannot be negligible.

Chapter 6

Crosstalk Digital Pre-Distortion

Digital Pre-Distortion for multi-antenna transmission chain brings with it coupling effects induced by the closely packed transmission chains running parallel to each other interacting closely with other transmission chains. Thus, digital pre-distortion should not only be the function of non-linearity and memory effects induced by PA of the same transmission chain but also it must be a function of distortion effects induced by parallelly running transmission chains. Coupling distortions i.e. crosstalk could be induced by different sections of transmission chain however here we have focused primarily on post PA crosstalk effects. These effects are brought by antenna coupling and mismatch effects or load modulation effects in advanced antenna array system. The new technique called Crosstalk Digital Pre-Distortion has been proposed here and has been observed to have considerable crosstalk cancellation effect as shown in the next chapter.
Following are prominent design features in the proposed algorithm:

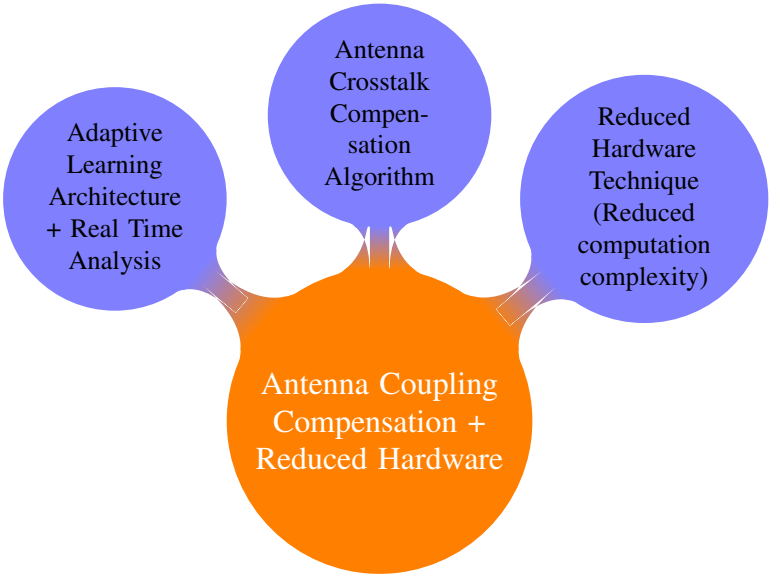

Figure 6.1: Design Features

The technique can be understood with the help of following flowcharts:
As can be seen, the model considers a single adaptive coefficient calculator block for multi

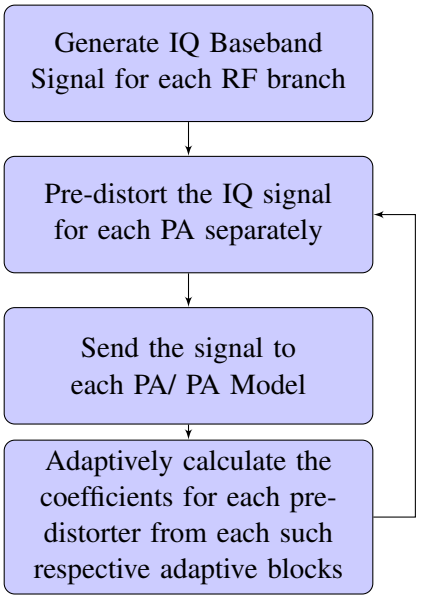

Figure 6.2: Flow Chart for conventional DPD

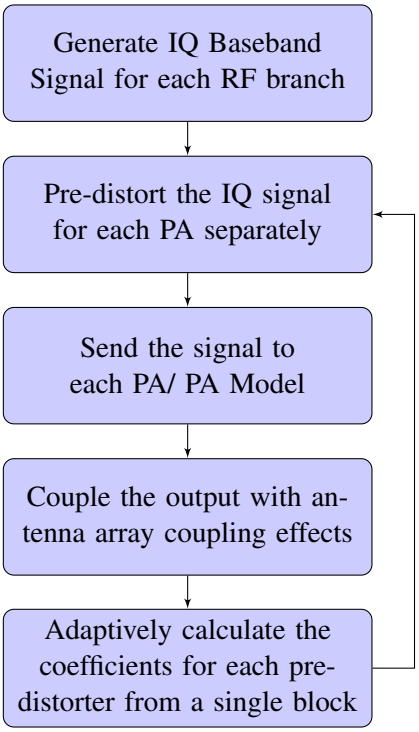

Figure 6.3: Flow Chart for CDPD

PA transmission paths instead of the traditional approach of having as many adaptive paths as the number of transmission paths simultaneously feeding each such respective PA pre-distorter. Further, the approach is particularly for antenna crosstalk compensation with pre-distortion algorithm adapting to crosstalk environment. However, the earlier approach did not consider the crosstalk effects. In addition to this only single pre-distorter with single input is required in open loop configuration operation of DPD.

Below is the Figure 6.6, a 4x1 transmission path has been modeled for the implementation of proposed CDPD technique and hence running the simulations. In the model, four IQ waveform generation sources are placed at the starting of each such transmission paths. These run simultaneously and fetch four desired signals for each of the branches. Further, each IQ waveform is pre-distorted by the DPD block taking a respective set of DPD coefficients calculated by single Adaptive Coefficient Calculator (ACC) block. Now each such pre-distorted waveform is sent to RF signal generator block which is supposed to amplify the IQ waveform with the desired gain and modulate the signal with RF wave. The signal is then sent to respective four PA Models extracted from the physical measurement setup of PAs. The output is then coupled with a noise source to model the noise from

adjacent systems in the environment. Then the signal from each such path is sent to "Coupler Antenna Array S Parameter Matrix" block Figure 6.4, to introduce post PA crosstalk effects. The "Coupler Block" is the modeling of antenna mismatch and coupling effects which is a set of s-parameter matrix extracted from the physical measurement setup of the 4x1 antenna array. Thus, it models the antenna array and coupling effects. Also, for simulation purpose, our own model of the s-parameter matrix could also be introduced to investigate coupling effects. The four outputs from the block are the coupled outputs required as feedback by Adaptive Coefficient Calculator (ACC) block to calculate the respective set of coefficients for each branch. The four outputs are also simultaneously fetched to four spectrum analyzers for measurement and analysis.

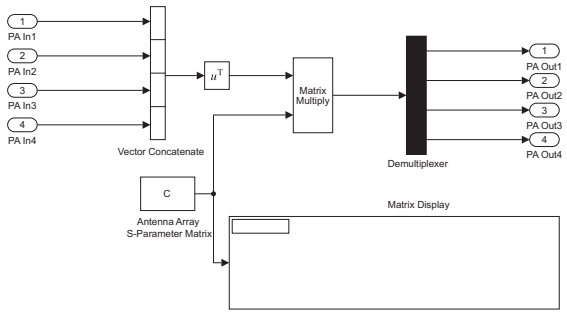

Figure 6.4: Coupler Architechture

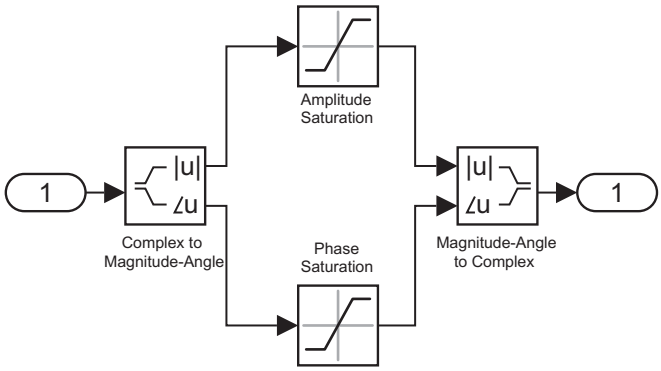

Figure 6.5: Clipper

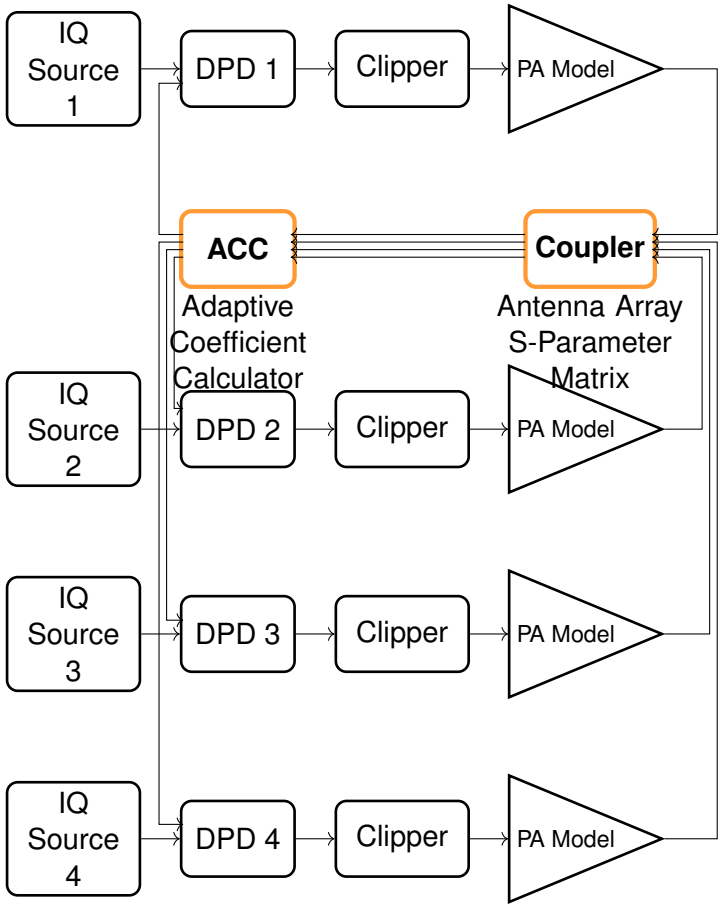

Figure 6.6: Hardware Model for Crosstalk DPD Algorithm 4x1 MIMO Simulations

Chapter 7
Measurement And Simulation Results

To investigate the problem of crosstalk distortions on the performance of power amplifier and transmitter output, two simulation models were created. To closely emulate the hardware implementation, models were created using Simulink. Further using HDL coder or Xilinx system generator tool, hardware model could be synthesized for digital predistortion implementation.

7.1 Simulation Models

Using Simulink, two simulation models were created to model the effects of post PA crosstalk and implementation of proposed compensation algorithm. Two transmission chain and four transmission chain models were created as shown in Chapter 6 with Saleh PA model[39] and MP PA Model as described in Chapter 3.

- 2x1 MIMO Simulation Model
- 4x1 MIMO Simulation Model

7.2 2x1 MIMO Simulation Model

Two transmission chains were designed with Saleh PA model[39] in place of PA model to mimic actual physical PA and rest design is similar to Figure 6.6 shown in Chapter 6, but only including two Tx paths. Two digitally beamformed LTE signals of 20 MHz bandwidth, 8 dB PAPR at 100 MHz sampling rate were fetched sample by sample to two path chains respectively in a cyclic repetition pattern. To better investigate the impact of crosstalk on power amplifier performances five different coupling scenarios were created. From a very low coupling of -23.01 dB, a low coupling of -16.99 dB, a medium coupling of -13.47 dB, a high coupling of -10.97dB to a very high coupling of -7.47dB were induced as shown in Table 7.1. Five coupling scenarios were tested with three different design configurations. First set of design run was conducted for 'without DPD' configuration i.e. no DPD running and coupling impacting directly PA outputs. Secondly, measurements were recorded 'with DPD' configuration. Finally, 'with CDPD' design was

introduced and observations were recorded. In the following sections, we will study the measurement results and observations from each case and finally conclude the outcome.

Coupling Scenario	Coupling Factor (S12)	Coupling Ratio (dB)
Very High	0.30 + 0.30i	-7.447
High	0.25 + 0.25i	-10.97
Medium	0.15 + 0.15i	-13.47
Low	0.10 + 0.10i	-16.99
Very Low	0.05 + 0.05i	-23.01

Table 7.1: 2x1 Tx Path Coupling Scenario

7.2.1 2x1 MIMO Results

7.2.1.1 Tx Paths Without DPD

Simulations to predict the effect of crosstalk and mismatch on radiated ACPR in MIMO scenario without DPD, i.e. coupling impacting directly PA outputs. Figure 7.1 and Table 7.2 shows the results for behaviour of PA for different levels of coupling. It can be observed ACPR is around -67 dB in all cases. There is hardly any impact on ACPR of output signal spectrum of each PA due to increment in coupling values. Here PA in TX2 branch outputs is shown. Crosstalk and mismatch are masked by PA nonlinearities, hence no impact of crosstalk visible on PA output spectrums.

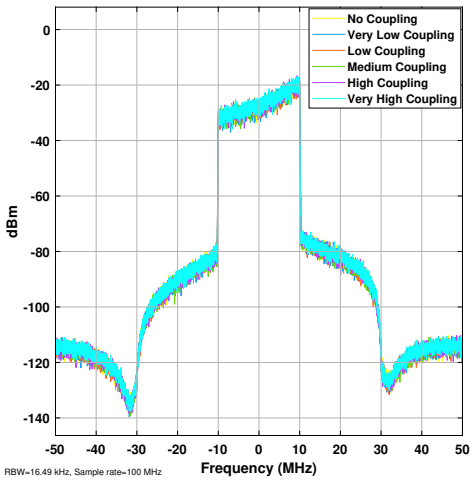

Figure 7.1: 2Tx Path Without DPD

Coupling Scenario	ACLR dB	
	Lower (dBc)	Upper (dBc)
Very High	-67.42	-59.63
High	-67.44	-59.50
Medium	-67.40	-59.68
Low	-67.45	-59.71
Very Low	-67.43	-59.62

Table 7.2: Tx Path Results Without DPD

7.2.1.2 Tx Paths With DPD

Simulations to predict the effect of crosstalk and mismatch on radiated ACPR in MIMO scenario with DPD, i.e. coupling impacting outputs with DPD for each Figure 7.2 and Table 7.3 shows the results for the behavior of DPD output for different levels of coupling. Distortion due to crosstalk/mismatch is clearly visible here. As the coupling level increases, distortion in DPD output ACLRs also raises. This can't be compensated for by regular DPD, it requires dedicated solution to solve the problem such as the proposed Crosstalk DPD.

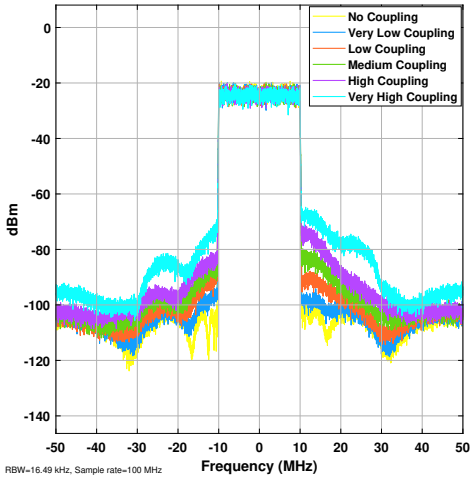

Figure 7.2: 2Tx Path With DPD

7.2.1.3 Tx Paths With CDPD

Simulations to predict the effect of crosstalk and mismatch on radiated ACPR in MIMO scenario with CDPD, i.e. coupling impacting CDPD outputs. Figure 7.3 and Table 7.4 shows the results for behavior of CDPD outputs for different levels of coupling. Distortion due to crosstalk/mismatch can be seen to be compensated by Crosstalk DPD.

Coupling Scenario	ACLR dB	
	Lower (dBc)	Upper (dBc)
Very High	-63.87	-54.51
High	-71.87	-63.92
Medium	-76.37	-70.07
Low	-80.00	-75.56
Very Low	-83.21	-81.10

Table 7.3: Tx Path Results With DPD

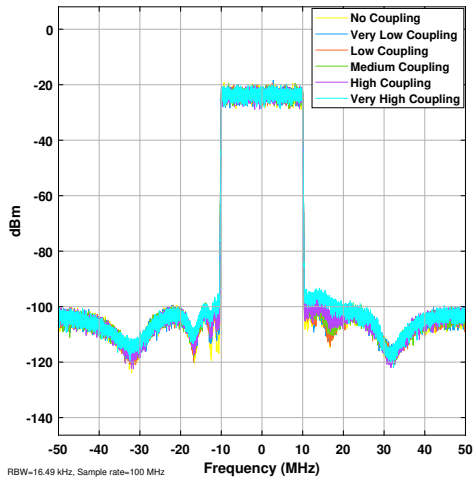

Figure 7.3: 2Tx Path With CDPD

Coupling Scenario	ACLR dB	
	Lower (dBc)	Upper (dBc)
Very High	-83.78	-79.49
High	-84.23	-82.50
Medium	-83.80	-82.94
Low	-83.88	-83.20
Very Low	-83.91	-82.96

Table 7.4: Tx Path Results With CDPD

7.2.1.4 Summarized Results

Observation: Varying Coupling degrades normal DPD ACLRs at each TX, which CDPD is successfully able to compensate. Table 7.5

Coupling Scenario	ACLR dB				
	Single Path		Two Path		
	No DPD	With DPD	No DPD	With DPD	With CDPD
Very High	-59.62	-82.90	-59.66	-54.51	-79.49
High	-59.62	-82.90	-59.50	-63.92	-82.50
Medium	-59.62	-82.90	-59.68	-70.07	-82.94
Low	-59.62	-82.90	-59.71	-75.56	-83.20
Very Low	-59.62	-82.90	-59.62	-81.10	-82.96

Table 7.5: Tx Path Summary Results

7.3 4x1 MIMO Simulation Model

To investigate crosstalk impact on multi-antenna transmission chain, 4x1 antenna model was developed. Hence three different coupling scenarios for 4x1 Antenna Array were created. These were high coupling scenario depicted in Table 7.6 to model high coupling impact, medium coupling by Table 7.7 for medium coupling impact and further a low coupling scenario shown in Table 7.8. Simulations were run with these different environments on the model shown on Figure 6.6 in Chapter 6. Observations and results are shown in Figure 7.4 and Figure 7.5 as the output spectrum from Tx1 and Tx2 respectively. The

High Coupling Matrix (4x1) dB				
Tx	Tx1	Tx2	Tx3	Tx4
Tx1	Tx11	-13.47	-16.99	-23.01
Tx2	-13.47	Tx22	-13.47	-16.99
Tx3	-16.99	-13.47	Tx33	-13.47
Tx4	-23.01	-16.99	-13.47	Tx44

Table 7.6: High Coupling Matrix (4x1) dB

Medium Coupling Matrix(4x1)dB				
Tx	Tx1	Tx2	Tx3	Tx4
Tx1	Tx11	-16.99	-23.01	-36.99
Tx2	-16.99	Tx22	-16.99	-23.01
Tx3	-23.01	-16.99	Tx33	-16.99
Tx4	-36.99	-23.01	-16.99	Tx44

Table 7.7: Medium Coupling Matrix (4x1) dB

spectrums are shown for high coupling scenario and only for two transmission chains. From both the spectrums it is visible how coupling impacts the outputs from both Tx chains. Yellow spectrums in both the plots are the PA input without any pre-distortion. It is also the IQ waveform signal uploaded for parallel running of four signal paths. The blue

Low Coupling Matrix (4x1) dB				
Tx	Tx1	Tx2	Tx3	Tx4
Tx1	Tx11	-23.01	-36.99	-56.99
Tx2	-23.01	Tx22	-23.01	-36.99
Tx3	-36.99	-23.01	Tx33	-23.01
Tx4	-56.99	-36.99	-23.01	Tx44

Table 7.8: Low Coupling Matrix (4x1) dB

colored output spectrums are the PA output showing out band distortions and in band distortions are clearly visible. Red spectrum is the normal DPD output without any crosstalk environment. Now, DPD is made to adapt to high coupling environment. The result of coupling is clearly seen as high out band distortions seen in the green spectrum. The level of distortions almost matches that of PA output curve. Now, in high coupling scenario CDPD algorithm is run and as can be seen in the violet curve the distortions have been compensated by the technique and ACLR levels have been restored to the previous values of normal DPD curve.

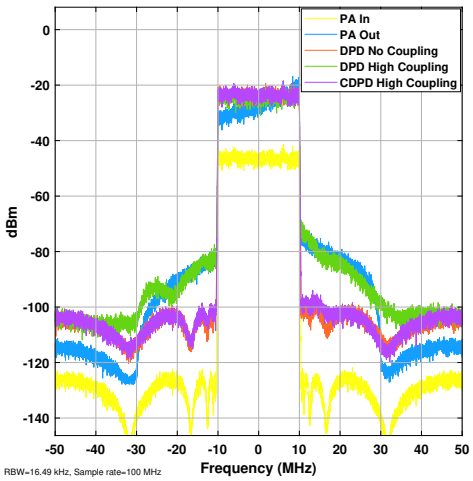

Figure 7.4: Tx 1

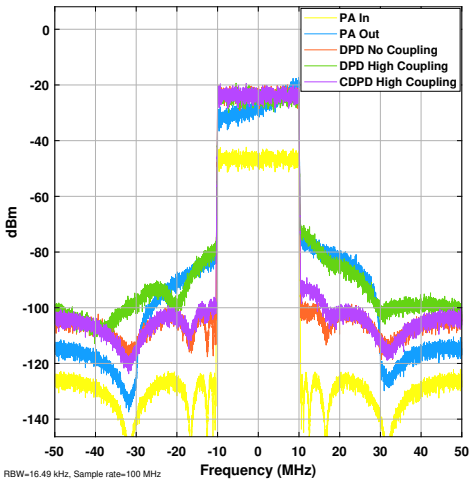

Figure 7.5: Tx 2

7.4 4x1 MIMO Results

In 4x1 Tx path model, PA models are replaced with four physical PA extracted models as discussed in Chapter 3. The model is run in three different coupling scenarios of high, medium, and very low given by the matrixes as discussed in the previous section. In these environments, the model is run for three different configurations to study the crosstalk impact. These are 'without DPD', 'with DPD' and 'with CDPD' algorithms. Output spectrum as observed is shown in following figures. Figure 7.6 and Figure 7.7

shows the PA 2 outputs and Rx output in without DPD configuration. Figure 7.8 and Figure 7.9 shows the PA 2 outputs and Rx output in with DPD configuration. Figure 7.10 and Figure 7.11 shows the PA 2 outputs and Rx output in with CDPD configuration.

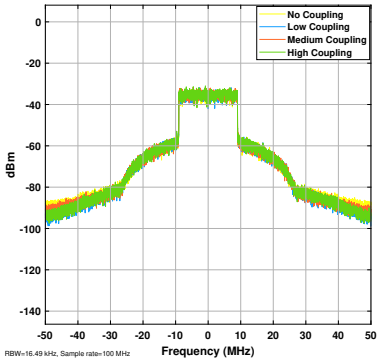

Figure 7.6: PA Output at Tx2

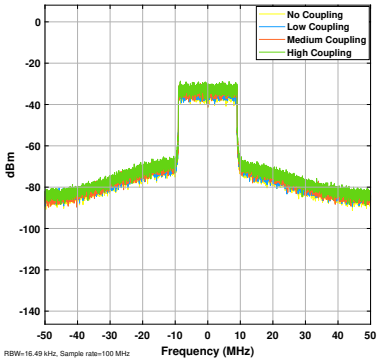

Figure 7.7: PA Output at Rx

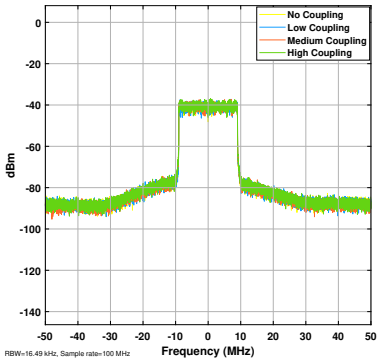

Figure 7.8: DPD Output Tx2

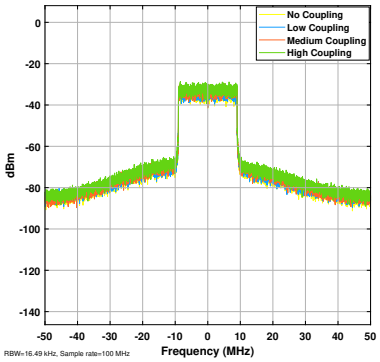

Figure 7.9: DPD Output Rx

Table 7.9 gives a summary of the results from above spectrums. It can be observed that DPD linearizes the distortions from PA output to DPD output at each of the Tx paths and Rx for all the coupling scenarios. The improvement is almost 9dB. However, the coupling has hardly any impact on either the output of PAs or at receiver without DPD running nor with DPD.

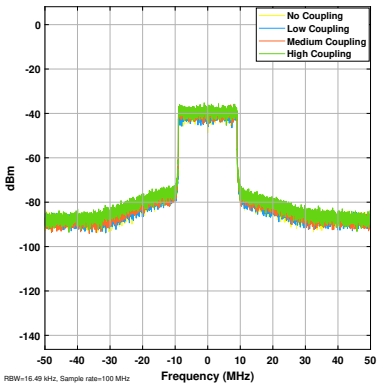

Figure 7.10: CDPD Output Tx2

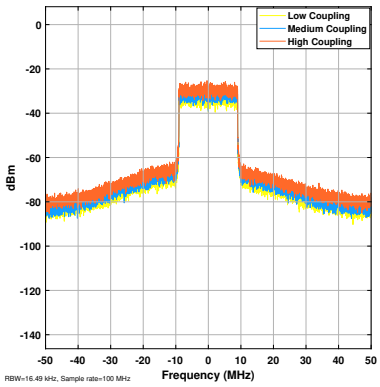

Figure 7.11: CDPD Output Rx

Without DPD					
Coupling Scenario	ACLR dBc				
	Tx1 Path	Tx2 Path	Tx3 Path	Tx4 Path	Rx of four Path
Nil	-32.71	-32.64	-33.54	-32.20	-32.70
Low	-32.61	-32.63	-33.56	-32.20	-32.75
Medium	-32.63	-32.59	-33.53	-32.20	-32.74
High	-32.71	-32.60	-33.55	-32.31	-32.76
With DPD					
Nil (DPD Output)	-41.50	-43.17	-39.65	-40.67	-41.26
Low	-41.66	-43.15	-39.63	-40.64	-41.24
Medium	-41.67	-43.42	-39.75	-41.07	-41.45
High	-41.58	-43.08	-39.84	-40.90	-41.44
With CDPD					
Low	-41.65	-43.05	-39.67	-40.74	-41.31
Medium	-41.69	-43.02	-39.16	-41.00	-41.45
High	-41.55	-43.36	-39.44	-40.93	-41.30

Table 7.9: 4x1 MIMO Summary Results

Chapter 8
Conclusion

An analysis of crosstalk effects focusing particularly on post PA crosstalk distortions on the performance of PA and or transmitted output signal was studied. Further, a Digital Pre-Distortion based approach was explored to solve post PA crosstalk distortions in multi-antenna transmitter system. To study the effects, a 4-antenna transmitter chain was developed in the measurement setup. The measurement setup was developed using four PAs from mini circuits and four PIFA antennas at the transmitting end. PAs were characterized and modeled using memory polynomial model so to be used in simulation models. The modeled PAs recorded quite good NMSE of -40 dB or less. Antenna array was synthesized for Digital Beamforming in a far-field scenario. Far-field for the 4x1 antenna array came out to be 1 m. For lateral sliding effects between antennas, antenna modules were designed, and 3D printed to investigate the effect of antenna coupling effects. To be able to emulate digital beamforming platform, four signal generators were configured for frequency synchronized phase stable, phase locked and phase controllable coherent configuration. To lock the phase, the local oscillator of a single synthesizer was shared between four signal generators.

To investigate the crosstalk effects in detail for various crosstalk environments and to emulate solution design from a hardware perspective, two models were designed in Simulink. 2x1 MIMO and 4x1 MIMO models were designed with the scope to study different crosstalk scenarios. Different PA models, Saleh, MP, and GMP models were also created and used to run simulations. Antenna array mismatch and coupling was extracted from the measurement set up in the form of an s-parameter matrix and modeled to introduce crosstalk effects in the simulation models. Further to investigate coupling effects deeper, five coupling scenarios were designed and tested for 2x1 MIMO model and three coupling scenarios for 4x1 MIMO model. The coupling impact was studied on PA outputs i.e. without DPD and then with DPD.

As observed from simulation results, the impact of post PA crosstalk was not found to be on the performance of PA but on the performance of DPD. For a very high coupling of the order of -7.44 dB, DPD performance is observed to degrade by 29 dB. At high coupling of -10.97 dB ACLR degraded by 20 dB and at the medium coupling of -13.47 dB, ACLR degradation was observed to be 13 dB. This degradation in ACLR is observed in closed loop adaptation of normal DPD algorithm in crosstalk environment. A Crosstalk Digital Pre-Distortion (CDPD) technique has been proposed to solve this problem of crosstalk on DPD performance. The technique was designed and implemented on the two models. Again, the coupling impact was studied on CDPD outputs in all previ-

ous coupling scenarios. An improvement is recorded to be 25 dB in very high crosstalk environment, 19 dB at the high coupling, 12 dB at the medium coupling and 8 dB in low coupling scenario. Hence, the proposed solution, CDPD is observed to successfully compensate for the crosstalk degradation in ACLR.

Chapter 9
Future Work

Several problems concerning limitation with measurement setup, antenna array design and interfacing sample-based simulation design of the solution algorithm with measurement setup are still unresolved and could, therefore, be addressed in future work on the topic.

The array antenna setup was not perfect as each element is placed individually without common plane at background making them susceptible to small planner fluctuations from their respective positions. Furthermore, array antenna was not designed in-house so a better control over its parameters was not possible. A simulation was done based on a theoretical element to compute parameters needed to build up an array.

Interfacing between the Simulink design of the solution algorithm and RF measurement setup was another major problem. The simulation model processed each sample of IQ data on a sample by sample basis. It also adapts in a closed loop configuration each iteration on per sample basis. However, RF signal generator which sends the signal to a power amplifier and spectrum analyzer which captures output signal from power amplifier both requires tens of thousands of samples in a file to be uploaded at a time. This creates a synchronization problem between simulation model and instrument setup which include physical model even if buffers are placed between them. This difference in latency and throughput requirements of the two system creates a problem in closed loop adaptation with the real system. Also, processing time (delay) of the physical setup fluctuates each iteration of closed loop adaption and particularly even more problematic when hundred thousand sample-based iteration is required for adaptation.

The same problem is posed even when MP or CTM PA models were used in the simulation model to extract pre-distorted signal or pre-distorter coefficients such that the signal could be recreated and fetched over physical PA setup. Still, the PA model is constant in nature which as they are extracted over the dynamic power range of signal generator but used at constant power in the simulation model. Thus, a closed loop adaptation is required between two systems at same time and throughput rate even when PA models are used to generate the pre-distorted signal. As a result, validation of the proposed method using measurement data could be done using script-based model rather than low throughput hardware model. The former approach will better synchronize with measurement setup and could be proposed as a future work.
The future work suggestions can be listed as the following:

- Antenna Array designing and analysis were evaluated for a linear four antenna array pattern. This could be done for more antenna array patterns such as 2X2

planner antenna array design.

- Measurement setup for real-time hardware analysis for crosstalk design could be built and interfaced to approve and confirm simulation results, further measurements for 2X2 planar array could also be approved.
- Hardware DPD pre-distortion for crosstalk compensation could further be implemented based on GMP model of pre-distortion in a closed loop adaptation.
- Transform Simulation-based HW model to script-based model to run the algorithm in closed loop adaptation with physical PA and instruments.
- Verification of proposed method using closed-loop measurement setup.
- Load-pull measurement setup to extract PA model to test performance under load modulation effects on DPD.
- Measurement and simulations using higher order MIMO array.

References

[1] *5G - Massive MIMO - MU-MIMO : ShareTechnote*. URL: http://www.sharetechnote.com/html/5G/5G_MassiveMIMO_MU_MIMO.html (visited on 05/01/2018).

[2] Abubaker Abdelhafiz et al. "A high-performance complexity reduced behavioral model and digital predistorter for MIMO systems with crosstalk". In: *IEEE Transactions on Communications* 64.5 (2016), pp. 1996–2004.

[3] Shoaib Amin et al. "Behavioral modeling and linearization of crosstalk and memory effects in RF MIMO transmitters". In: *IEEE transactions on microwave theory and techniques* 62.4 (2014), pp. 810–823.

[4] *Antenna Arrays (Phased Arrays)*. Accessed: 2018-04-29. URL: http://www.antenna-theory.com/arrays/main.

[5] *Antenna measurement theory orbit fr*. URL: http://www1.isti.cnr.it/~salerno/Microonde/Intro_Ant_meas.pdf (visited on 05/11/2018).

[6] Filipe M Barradas, Telmo R Cunha, and Jose C Pedro. "Digital predistortion of RF PAs for MIMO transmitters based on the equivalent load". In: *Integrated Nonlinear Microwave and Millimetre-wave Circuits Workshop (INMMiC), 2017*. IEEE. 2017, pp. 1–4.

[7] Seyed Aidin Bassam, Mohamed Helaoui, and Fadhel M Ghannouchi. "Crossover digital predistorter for the compensation of crosstalk and nonlinearity in MIMO transmitters". In: *IEEE transactions on microwave theory and techniques* 57.5 (2009), pp. 1119–1128.

[8] Sergio Benedetto, Ezio Biglieri, and Riccardo Daffara. "Modeling and performance evaluation of nonlinear satellite links-a Volterra series approach". In: *IEEE Transactions on Aerospace and Electronic Systems* 4 (1979), pp. 494–507.

[9] XAVIER BLAND. "Modeling of Power Amplifier Distortion in MIMO Trans-mitters". In: *Master thesis* (2013).

[10] R Neil Braithwaite. "Wide bandwidth adaptive digital predistortion of power amplifiers using reduced order memory correction". In: *Microwave Symposium Digest, 2008 IEEE MTT-S International*. IEEE. 2008, pp. 1517–1520.

[11] *Cisco Visual Networking Index: Global Mobile Data Traffic Forecast Update, 2016–2021 White Paper - Cisco*. URL: https://www.cisco.com/c/en/us/solutions/collateral/service-provider/visual-networking-index-vni/mobile-white-paper-c11-520862.html (visited on 05/11/2018).

[12] Kevin Clifton. *Advanced PA Test Techniques :National Instrument*. URL: ftp://ftp.ni.com/pub/branches/uk/ats_2014/Power_Amplifier_Testing.pdf (visited on 05/12/2018).

[13] Lei Ding et al. "A robust digital baseband predistorter constructed using memory polynomials". In: *IEEE Transactions on communications* 52.1 (2004), pp. 159–165.

[14] Lei Ding et al. "Memory polynomial predistorter based on the indirect learning architecture". In: *Global Telecommunications Conference, 2002. GLOBECOM'02. IEEE*. Vol. 1. IEEE. 2002, pp. 967–971.

[15] David Gesbert et al. "Shifting the MIMO paradigm". In: *IEEE signal processing magazine* 24.5 (2007), pp. 36–46.

[16] Fernando Gregorio et al. "Power amplifier linearization technique with IQ imbalance and crosstalk compensation for broadband MIMO-OFDM transmitters". In: *EURASIP Journal on Advances in Signal Processing* 2011.1 (2011), p. 19.

[17] Katharina Hausmair. "Modeling and Compensation of Nonlinear Distortion in Multi-Antenna RF Transmitters". In: (2018).

[18] Katharina Hausmair et al. "Digital Predistortion for Multi-Antenna Transmitters Affected by Antenna Crosstalk". In: *IEEE Transactions on Microwave Theory and Techniques* 66.3 (2018), pp. 1524–1535.

[19] Hon Tat Hui, Marek E Bialkowski, and Hoi Shun Lui. "Mutual coupling in antenna arrays". In: *International Journal of Antennas and Propagation* 2010 (2010).

[20] Sean Victor Hum. *ECE 422 - Radio and Microwave Wireless Systems*. URL: http://www.waves.utoronto.ca/prof/svhum/ece422/notes/15-arrays2.pdf (visited on 05/01/2018).

[21] Tao Jiang. "Behavioral modeling and FPGA implementation of digital predistortion for RF and microwave power amplifiers". PhD thesis. Politecnico di Torino, 2016.

[22] W. Kabir. "Orthogonal Frequency Division Multiplexing (OFDM)". In: *2008 China-Japan Joint Microwave Conference*. Sept. 2008.

[23] J Kim and K Konstantinou. "Digital predistortion of wideband signals based on power amplifier model with memory". In: *Electronics Letters* 37.23 (2001), pp. 1417–1418.

[24] Ms.Varsharani Mokal, Prof S.R. Gagare, and Dr.R.P. Labade. "Analysis of Micro strip patch Antenna Using Coaxial feed and Micro strip line feed for Wireless Application". In: *IOSR Journal of Electronics and Communication Engineering* 12 (June 2017), pp. 36–41.

[25] Dennis R Morgan et al. "A generalized memory polynomial model for digital predistortion of RF power amplifiers". In: *IEEE Transactions on signal processing* 54.10 (2006), pp. 3852–3860.

[26] Ralf R Müller, Mohammad A Sedaghat, and Georg Fischer. "Load modulated massive MIMO". In: *Signal and Information Processing (GlobalSIP), 2014 IEEE Global Conference on*. IEEE. 2014, pp. 622–626.

[27] Om Prakash Nandi. *Behavioral Modeling of Power Amplifier with Memory Effect and Linearization Using Digital Pre Distortion*. University of Gävle, Sweden, 2016.

[28] 3rd Generation Partnership Project Technical Specification Group Radio Access Network. *Evolved Universal Terrestrial Radio Access (E-UTRA); Physical channels and modulation (Release 14)*. Version Technical specification 3GPP TS 36.211 V15.1.0. Mar. 2018.

[29] Mohamed K Nezami. "Fundamentals of power amplifier using digital predistortion". In: *High Frequency Electronics* 54 (2004), p. 59.

[30] Conor O'keeffe and Joe Moore. *Wireless network element and method for antenna array control*. US Patent 9,525,204. Dec. 2016.

[31] Y. Palaskas et al. "A 5-GHz 108-Mb/s 2 $times$2 MIMO Transceiver RFIC With Fully Integrated 20.5-dBm rmP_{rm1dB} Power Amplifiers in 90-nm CMOS". In: *IEEE Journal of Solid-State Circuits* 41.12 (Dec. 2006), pp. 2746–2756.

[32] F. H. Raab et al. "Power amplifiers and transmitters for RF and microwave". In: *IEEE Transactions on Microwave Theory and Techniques* 50.3 (2002), pp. 814–826.

[33] Victor Rabinovich and Nikolai Alexandrov. "Typical Array Geometries and Basic Beam Steering Methods". In: *Antenna Arrays and Automotive Applications*. Springer New York, 2013, pp. 23–54.

[34] Chiara Ramella et al. "High Efficiency Power Amplifiers for Modern Mobile Communications: The Load-Modulation Approach". In: *Electronics* 6.4 (2017), p. 96.

[35] Schwarz Rohde. "Generating Multiple Phase Coherent Signals – Aligned in Phase and Time". In: (), p. 73. URL: http://www.rohde-schwarz.com/appnote/1GP108 (visited on 05/26/2018).

[36] Schwarz Rohde. "Millimeter-Wave Beamforming: Antenna Array Design Choices & Characterization". In: 2016. URL: http://www.rohde-schwarz.com/appnote/1MA276 (visited on 05/26/2018).

[37] M Romier et al. "Load-Pull Effect on Radiation Characteristics of Active Antennas". In: *IEEE Antennas and Wireless Propagation Letters* 7 (2008), pp. 550–552.

[38] Mohammed Al-Sadoon et al. "Weight optimization for adaptive antenna arrays using LMS and SMI algorithms". In: *WSEAS Trans. Commun* 15 (2016), pp. 206–214.

[39] Adel AM Saleh. "Frequency-independent and frequency-dependent nonlinear models of TWT amplifiers". In: *IEEE Transactions on communications* 29.11 (1981), pp. 1715–1720.

[40] Martin Schetzen. "The Volterra and Wiener theories of nonlinear systems". In: (1980).

[41] Dominique Schreurs et al. *RF power amplifier behavioral modeling*. Cambridge University Press New York, NY, USA, 2008.

[42] Ibrahim Can Sezgin. "Different Digital Predistortion Techniques for Power Amplifier Linearization". In: (2016).

[43] MN Md Tan et al. "Smart antenna: weight calculation and side-lobe reduction by unequal spacing technique". In: *RF and Microwave Conference, 2008. RFM 2008. IEEE International*. IEEE. 2008, pp. 441–445.

[44] Michal Vavrda. "Digital beamforming in wireless communications". In: *Brno University of Technology* (2011).

[45] Hossein Zargar, Ali Banai, and José C Pedro. "A new double input-double output complex envelope amplifier behavioral model taking into account source and load mismatch effects". In: *IEEE Transactions on Microwave Theory and Techniques* 63.2 (2015), pp. 766–774.